CHALMERS

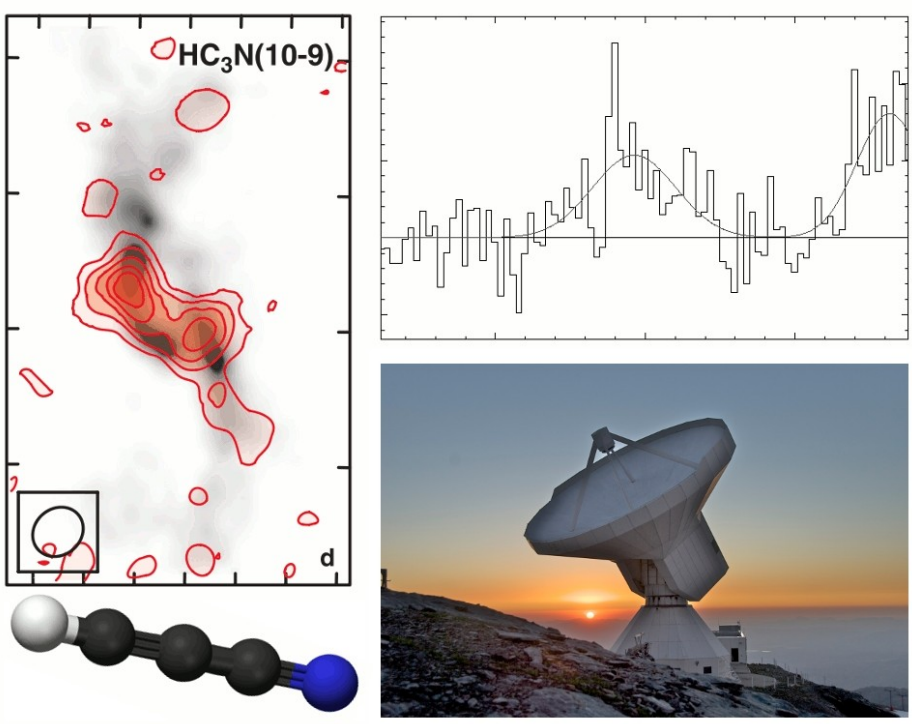

Image credit (clockwise, starting at top left): Meier & Turner 2005 (HC_3N map in IC 342); This work (HC_3N spectrum in IRAS 17208-0014); Rebus/IRAM (IRAM 30 m telescope); Wikimedia Commons (HC_3N molecule).

HC_3N as a Diagnostic Tool for Activity in Galaxies

Master of Science Thesis in Radio and Space Science

JOHAN LINDBERG
Supervisor: Susanne Aalto

Department of Radio and Space Science
Onsala Space Observatory
CHALMERS UNIVERSITY OF TECHNOLOGY
Göteborg, Sweden, 2009

HC_3N as a Diagnostic Tool for Activity in Galaxies

Johan Lindberg

Department of Radio and Space Science
Onsala Space Observatory
CHALMERS UNIVERSITY OF TECHNOLOGY
Göteborg, Sweden, 2009

HC_3N as a Diagnostic Tool for Activity in Galaxies

Department of Radio and Space Science
Chalmers University of Technology
SE-439 92 Onsala
Sweden
Telephone: +46 (0)31-772 5500

Department of Radio and Space Science, Onsala, 2009

Abstract

The aim of this thesis is to discuss a small survey of extragalactic measurements of HC_3N, as well as present results of unpublished HC_3N measurements in galaxies. These data have been compared with HCN and HNC data from the literature and from new observations, thus giving estimates of line ratios between these three molecules in about 15 galaxies. This can help understanding the evolution of active galaxies, and also make it easier to distinguish galaxies powered by starbursts from those powered by active galactic nuclei (AGN).

Our spectral line observations have been made with the IRAM, SEST, OSO 20 m and JCMT telescopes between 2001 and 2008.

Among the new HC_3N data, detections of HC_3N in six galaxies with no earlier detections are reported. Three new detections of HNC and one new detection of HCN are also reported. The detection of HC_3N in IRAS 17208-0014 is the most distant detection of this molecule yet reported.

The formation of HC_3N is discussed, and the theory that HC_3N is formed from C_2H_2 on the grains reacting with CN is supported by the data.

The HC_3N line ratios are compared with other parameters important to star formation and AGN activity. A tentative correlation between HC_3N and PAH (polycyclic aromatic hydrocarbons) emission is reported, as well as a tentative correlation between HC_3N and the depth of silicate absorption.

A preliminary definition "HC_3N-luminous galaxy", based on the HC_3N/HCN ratio, is made, and most HC_3N-luminous galaxies seem to be galaxies with deeply obscured cores and (U)LIRGs – (ultra-)luminous infrared galaxies. Many of them also seem to have OH megamaser activity. A possible explanation is that both HC_3N and OH megamasers need warm dust for their excitation. Alternatively, the dust offers protection against UV destruction.

This work will be adapted into an article for Astronomy & Astrophysics during the autumn/winter of 2009.

KEYWORDS: galaxies: ISM – galaxies: starburst – galaxies: active – radio lines: galaxies – radio lines: ISM – ISM: molecules – molecules: HC_3N

Sammanfattning

Målet med rapporten är att presentera en mindre observationell kartläggning av extragalaktiska mätningar av HC_3N, samt att redovisa data från tidigare ej publicerade HC_3N-mätningar i galaxer. Dessa data har jämförts med HCN- och HNC-data både från litteraturen och från nya observationer. Med detta har linjekvoter mellan dessa molekyler kunnat uppskattas i cirka 15 galaxer. Detta kan bidra till förståelsen av aktiva galaxers utveckling och även underlätta arbetet att skilja på aktiva galaxer som drivs av starbursts från de som drivs av aktiva galaxkärnor (AGN:er).

Våra spektrallinjemätningar har utförts med teleskopen IRAM, SEST, OSO 20 m och JCMT mellan åren 2001 och 2008.

I de nya HC_3N-mätningarna återfinns HC_3N-detektioner i sex galaxer där molekylen inte detekterats tidigare. Tre nya HNC-detektioner och en ny HCN-detektion rapporteras också. Detektionen av HC_3N i IRAS 17208-0014 är den mest avlägsna detektionen av denna molekyl som någonsin gjorts.

Processen som bildar HC_3N diskuteras, och teorin att HC_3N bildas ur C_2H_2 på stoftkorn som reagerar med CN stöds av nya data.

HC_3N-linjekvoterna jämförs med andra parametrar som är viktiga för stjärnbildning och AGN-aktivitet. En tentativ korrelation mellan HC_3N och emission från PAH (polycykliska aromatiska kolväten) rapporteras, så även en tentativ negativ korrelation mellan HC_3N och silikatabsorption.

En preliminär definition av "HC_3N-luminös galax"föreslås med utgångspunkt från HC_3N/HCN-linjekvoterna. De flesta HC_3N-luminösa galaxer verkar vara galaxer med djupt stoftbegravda kärnor och (U)LIRG:er – (ultra-)luminösa infraröda galaxer. Många av dem verkar också ha OH-megamaseraktivitet. En möjlig förklaring är att både HC_3N och OH-megamasrar behöver varmt stoft för att exciteras. En annan möjlighet är att stoftet skyddar mot UV-strålning.

Detta arbete kommer att omarbetas till en artikel i Astronomy & Astrophysics under hösten/vintern 2009.

Nyckelord: galaxer: interstellärt medium – galaxer: starburst – galaxer: aktiva – radiolinjer: galaxer – radiolinjer: interstellärt medium – interstellärt medium: molekyler – molekyler: HC_3N

Preface

"Look for the bare necessities
The simple bare necessities
Forget about your worries and your strife
I mean the bare necessities
Old Mother Nature's recipes
That brings the bare necessities of life"
The bear Baloo in Walt Disney's *The Jungle Book*

In this thesis, a survey of HC_3N in external galaxies is presented. All extragalaxtic HC_3N measurements found in the literature as well as until now unpublished data are included. The possibility of using HC_3N as a tracer for activity in galaxies is discussed.

Chapter 1 is a general introduction to the field of radio astronomy and astrochemistry. In Chapter 2, the basic theory of molecular spectroscopy is introduced. Chapter 3 contains descriptions of the most important molecules in astrochemistry, as well as a discussion of possible formation processes. Then, in Chapter 4, the properties and structure of active galaxies (AGN galaxies and starburst galaxies) are discussed.

The methods of observation as well as the selection of the sample of galaxies is discussed in Chapter 5. This chapter also contains a few words about classification of these objects, as well as short descriptions of each galaxy in the sample. In Chapter 6, the results of the measurements as well as the data found in the literature are shown. Also, the calculations of line ratios are accounted for, and the results of these calculations are listed. Chapter 7 contains a short discussion on erroneous line ratios in the most nearby galaxies.

Chapter 8 contains a discussion on possible correlations between HC_3N luminosity and other galaxy properties. Then, in Chapter 9, calculations on the possibility of the HC_3N intensity being pumped are shown. Finally, Chapter 10 summarises the results of this thesis project.

There are also a few appendices to the thesis. In Appendix A, some oddities in different measurements on the same objects are discussed. In Appendix B the difficulty of separating AGN galaxies from starburst galaxies are shown by comparing different parts of the literature. Appendix C contains the spectra of all measurements reported in this work. Appendix D contains a small bestiary of the molecules discussed in the thesis. Finally, Appendix E contains a recipe used for the data reduction in this work.

Acknowledgements

When I started this work, I knew the simple basics of radio astronomy, and also some basic spectroscopy and quantum physics. Thanks to my supervisor, Susanne Aalto, I have gained lots of knowledge about the use of molecular radio astronomy and astrochemistry as tools for analysing space. She has been encouraging, helpful and able to explain the deep jungle of astrochemistry as well as many other aspects of astrophysical research. I am very happy for asking her for a thesis project, as I have gained so much knowledge and skills during these six months.

Also, many thanks to Francesco Costagliola, Susanne's PhD student, who has always been very supportive, friendly and positive. It's always fun to work with Francesco. I especially want to thank him for his help on the calculations regarding radiative excitation and pumping, but also for all support and encouragement. I also thank him for trusting me with his valuable observation time at the IRAM telescope – I learned a lot from going there. This is just one example of why I have felt so welcome by this small team of researchers.

I also want to thank everyone who has provided data for this project: Thomas R. Greve, Rossa Hurley, Sergio Martín Ruiz, Raquel R. Monje, Sebastien Muller, Juan-Pablo Pérez-Beaupuits, Henrik W. W. Spoon, Martina C. Wiedner, and of course Francesco Costagliola and Susanne Aalto.

Many thanks to Per Bergman for help with installing and running `xs` on my new Ubuntu system, which wasn't as easy as it sounds.

To Monica Rodriguez and Fabien Batejat, for good help and company while at the IRAM, and also to the astronomer and operators at IRAM for all your invaluable help: Hans Ungerechts, Joaquín Santiago, Ignacio Ruiz and Breezy Ocana.

To all friends at Onsala Space Observatory, in particular the PhD students who were my company in the Space Bus and in the PhD room: Daniel, Per, Rossa, Fabien, Francesco and Simon.

To all my friends in the Chalmers Baroque Ensemble, without whom I wouldn't be what I am today. Thanks for all fun parties, tours, concerts, rehearsals, expotitions, etc.

To my parents, Solveig and Håkan, for your love and support. You have always been there for me.

Finally, all my love to Ylva. Thanks for your love, devotion and patience during my work with this project.

Santa Cruz de La Palma, October 13, 2009
JOHAN LINDBERG

CONTENTS

1 INTRODUCTION

The first detection of spectral lines in astronomy was made by Joseph von Fraunhofer in 1814, when absorption lines were discovered in the Sun's spectrum (Fraunhofer 1822, Tennyson 2005). Karl Jansky made the first discovery of a non-terrestrial radio signal in 1931 (Jansky 1933, Rohlfs & Wilson 2004). In the late 1930s, W. S. Adams discovered optical transitions of CH and CN, which were the first detections of molecules in space (Adams 1941).

The first radio astronomical discovery of a molecule was made in 1963, when two OH absorption lines were discovered in the supernova remnant Cassiopeia A (Barrett et al. 1964, Rohlfs & Wilson 2004). Since then, more than a hundred different molecules have been discovered in our Galaxy, most in the radio spectrum. Almost 40 of these have also been found in extragalactic objects (other galaxies).

The observations in our own galaxy, the Milky Way (hereafter referred to as "the Galaxy"), have been made both in stars, nebulae and in the interstellar medium – the gas and dust in the space between the stars. Regions with dense molecular gas in the interstellar medium might eventually evolve into star forming regions, which is why the study of the dense gas in galaxies is of certain interest to astronomers.

When studying molecular lines in external galaxies, the sizes of the observed objects are too small to distinguish single stars, or even single gas clouds. Excluding the few nearest galaxies, all single-dish[1] extragalactic measurements on molecular lines in the radio or sub-millimetre (sub-mm) spectra will measure the molecular contents of the whole galaxy due to the low resolution (large beam size) of the telescopes being used. Note that the resolution is higher than the galaxies' extension in the optical spectrum, but that the molecular gas is concentrated to small regions in the centres of the galaxies. Galaxies subtending several arcminutes in the optical spectrum might only have dense molecular gas in the central 10-20 arcseconds. Translated to real distances, the galaxy could have a diameter of 20-30 kpc[2] in the optical spectrum, but the dense molecular gas might be inside a region only 1-2 kpc across.

If a higher resolution is desired, interferometry – the use of several single-dish telescopes to form an array of telescopes – can be used. This way, the main features of the molecular distribution in a galaxy can be measured.

Molecular spectroscopy is obviously used to investigate the chemical composition of distant objects, but it can also be used to determine properties such as temperature, density and pressure.

CO is by many considered to be the most important molecule for tracing molecular gas in the interstellar medium. Due to its low dipole moment, it has a low critical density, which means that it can be used to trace gas clouds with rater low densities ($10^2 - 10^3$ cm^{-3}) – the collision partner (H_2) density needed for CO emis-

[1]Measurements performed with a single radio telescope, in contrast to interferometry, which uses several radio telescopes to simulate telescopes much larger than what can be constructed.

[2]kpc = kiloparsec, 1 pc = 3.26 lightyears.

sion to show up is lower than for most other molecules. Other molecules with higher dipole moments, such as HCN, HNC and HCO^+, are used to trace denser molecular gas ($> 10^4$ cm^{-3}), as these will require a higher H_2 density to be detected.

Among the largest molecules found in space identified by spectroscopic lines are the cyanopolyynes, HC_xN, where $x = 3, 5, 7, ...$, thus being carbon chains of different lengths with an attached cyano-group (CN). It shall be noted that larger molecules such as PAHs (polycyclic aromatic hydrocarbons) have been identified in space, but by broad emission bands consisting of the spectral features of several similar PAH molecules, rather than narrow spectral lines specific to certain molecules.

In this report, a survey in extragalactic sources for the simplest cyanopolyyne HC_3N is documented. The importance of this molecule when investigating the properties of dust-enshrouded galaxies is presented, the chemistry forming HC_3N is discussed, and possible correlations with (other) indicators of star-formation activity are investigated.

2 MOLECULAR SPECTROSCOPY

In spectroscopy, the unique fingerprints of electromagnetic radiation emitted and absorbed by all atoms and molecules are studied. This way, not only the chemical composition of a distant region can be investigated, but also e.g. its temperature, pressure, density and velocity.

2.1 Rotational transitions

In quantum physics, we learn that the energies of atoms and molecules can only take on certain quantised (discrete) energy levels. The atoms or molecules can, following more or less strict rules, change their energy state. To be able to change to a higher energy level, the extra energy must be provided externally, e.g. from a photon or by collision with another atom/molecule. When the atom or molecule (spontaneously) shifts to a lower state, a photon carrying the exact energy difference between the two levels will be emitted. Many such photons will together create one of the lines in the spectral fingerprint of the atom or molecule.

Most of the molecular transitions discussed in this text are transitions between rotational levels, meaning an abrupt change of the quantum angular momentum J. For radiatively induced transitions, only transitions where J is increased or decreased by the number 1 are allowed ($\Delta J = \pm 1$) (Barrow 1962). For collisionally induced transitions, no such selection rule apply, but transitions with $\Delta J = \pm 1$ and $\Delta J = \pm 2$ are favoured (Carroll & Goldsmith 1981), and transitions as high as $\Delta J = \pm 6$ should be possible (Draine 1985).

In this text – if not stated otherwise – all transitions discussed should be understood as rotational transitions, meaning that the "HC_3N 10-9 transition" should be interpreted as the transition for which an HC_3N molecule changes its quantum angular momentum J from the value 10 to the value 9.

Most molecular rotational transitions require/provide energies equivalent to photons in the radio spectrum (mostly mm or sub-mm waves). Note that molecules need a permanent dipole moment to have different rotational states, meaning that they need to be asymmetric – thus, common symmetric molecules like H_2, O_2 and CO_2 show no rotational transitions.

2.2 Vibrational transitions

Molecules do not only have rotational energy states, but also vibrational energy states, defined by different quantum vibrational energies. One possible kind of vibration takes place when the atoms move back and forth towards each other, like two masses attached to a spring. For polyatomic molecules (molecules with at least three atoms), vibrations can also occur as a bending around one (or several) of the atoms in the molecule, somewhat like a hinge opening and closing. As the energy differences between the vibrational states are much larger than the differences between the rotational states, a lot more energy needs to be provided to cause a

vibrational transition instead of a rotational transition. Thus, vibrational transitions induced by collisions need a much higher abundance of collision partners or a much higher temperature (higher velocity of the collision partners).

For radiatively induced transitions, much more energetic radiation (i.e. infrared radiation) is needed instead of mm-radiation, and the following selection rule applies: $\Delta v = \pm 1$, where v is the vibrational level. Normally, a vibrational transition also changes the rotational level with the selection rule $\Delta J = \pm 1$, however, exceptions to this rule are possible. For a more extensive discussion, refer to e.g. Barrow (1962) or Tennyson (2005).

2.3 IR pumping of spectral lines

A strong IR source may cause vibrational transitions in a population of molecules. However, it might also affect the excitation in rotational energy levels. If the abundance of collision partners giving rise to the rotational transitions (in most cases hydrogen molecules, H_2) is very low, the vibrational excitations induced by the IR source will be more effective than the spontaneous rotational decays. This creates a "pumping" phenomenon: For a vibrational transition, there is mostly also a change in J by 1 (see above), thus making it possible for J to increase by 2 if a molecule is vibrationally excited, and then falls back into the vibrational ground state ($v = 0$). If this molecule is once more excited by the IR source before it has decayed down to $J = 0$, the IR source will make the molecules achieve higher and higher rotational states via high vibrational states. This is called infrared pumping. (Carroll & Goldsmith 1981)

The name of the phenomenon comes as the IR source raises, or "pumps", the molecules to rotational levels much higher than what would have been expected only considering the rotational transitions induced by collisions or sub-mm radiation. If the pumping is disregarded, temperatures and other properties calculated from the line intensities might be severely affected.

2.4 The shape of spectral lines

Rather than being narrow spikes, spectral lines from extragalactic sources extend to a certain width on the frequency axis. This is not caused by quantum uncertainty, but rather by the signals being emitted by gas clouds moving around inside the galaxy, causing Doppler broadening of the lines. Before explaining this, we first note that the central frequency of the spectral line will be Doppler shifted, as most galaxies are moving away rapidly from our Galaxy. The most distant galaxy in the sample, IRAS 17208-0014 (the sample will be discussed in Chapter 5), has a redshift of $z = 0.043$, making a signal emitted at the frequency 90 GHz shifted to 86 GHz as seen from the Galaxy. This redshift corresponds to a velocity of around 12,800 km/s. However, as the galaxies are rotating around their own axes, the velocity difference between the parts of the dense gas rotating towards us and the parts rotating away from us can be several hundred km/s, thus creating broad spectral peaks.

If the dense gas in the galaxy is distributed as a Gaussian, the peak will also be a

Gaussian. If the spectrum can not be fitted to one Gaussian, but instead to two (or several) well-separated Gaussians, this could indicate that the molecular gas in the galaxy consists of two (or several) separate parts, maybe being merged together into one galaxy. One of many other possibilities is that the molecular gas is distributed in a ring around the centre of the galaxy.

3 MOLECULES IN ASTRONOMY

The most abundant molecule in the universe is molecular hydrogen, H_2. However, since it has no dipole moment, it has no rotational transitions, and thus cannot be detected by radio/mm spectroscopy. Hot H_2 gas, for which $T \gtrsim 100$ K, however, show vibrational transitions in the IR spectrum.

About 150 different molecules have been found in space (in the interstellar medium or in circumstellar shells), most of them identified by their rotational and/or vibrational spectra. Below, the molecules most important in this work will be discussed, namely CO, HCN, HNC, HC_3N, C_3N, C_2H_2 and C_2H. Other molecules commonly found in the universe are e.g. H_2O, HCO^+, CS, OH, NH_3 and CN.

3.1 CO

CO (carbon monoxide) is the most easily detected molecule in the mm-spectrum, since it is the most abundant molecule with a non-zero dipole moment, and the second most abundant molecule in the universe after H_2 (Tennyson 2005). It is thus used instead of H_2 to trace cold molecular gas, since the CO 1-0 transition is triggered by collisions between CO and H_2.

Much work has been put into determining a conversion factor between the CO 1-0 intensity and the H_2 density. A good assumption is that $n(\mathrm{CO}) \sim 10^{-4} n(\mathrm{H_2})$ (Tennyson 2005). A more extensive discussion of the use of CO as a tracer of H_2 can be found in Scoville & Sanders (1987).

3.2 HCN and HNC

Among the more abundant molecules in the interstellar gas are HCN and its isomer HNC. HCN is more commonly known on Earth as hydrogen cyanide, and is an extremely poisonous liquid. In space, it is one of the most common tracers of dense interstellar gas.

HCN's isomer HNC (hydrogen isocyanide) can be created from HCN at low temperatures by neutral-neutral reactions with neutral hydrogen: HCN + H $\longrightarrow$ H + HNC, and HNC can be transferred into HCN at high temperatures following the opposite reaction (Aalto et al. 2002).

HCN is one of the most important tracers of dense gas (see e.g. Papadopoulos (2007)). The critical density of a rotational transition determines the perturber density above which collisional excitations dominate the excitations of the transition. Here, the perturber mostly is H_2, since it is by far the most abundant molecule anywhere in the universe. The critical density $n_{\mathrm{crit}} \propto \mu^2 \nu^3_{J+1,J}$ (Papadopoulos 2007), where μ is the dipole moment of the molecule. Since HCN has much larger dipole moments than CO (2.98 D for HCN, 0.11 D for CO (Papadopoulos 2007)), its critical density for rotational transitions is much higher than the critical density of CO, making it a tracer of gas 300 times more dense than gas traced by CO.

Even if dense gas is an important component for star formation (Meier & Turner

2005), it is not clear whether a high HCN abundance in a galaxy definitely indicates massive star formation, or if an AGN in the centre of the galaxy also could be responsible for the accumulation and heating of the gas. The HNC/HCN ratio can possibly tell something about where the dense gas comes from, as overluminous HNC emission ($I(\mathrm{HNC})/I(\mathrm{HCN}) > 1$) may indicate that the chemistry is affected by X-rays (Aalto 2008), while low HNC emission could be a sign of shocks (Schilke et al. 1992).

3.3 HC_3N

A major part of what we know about HC_3N (sometimes written HCCCN or C_3HN), also known as cyanoacetylene, comes from studies of molecules in space. HC_3N is not a particularly common molecule on the Earth, nor is it one of the most studied astromolecules. It has been discovered in some objects in the solar system, e.g. Saturn's moon Titan (Sagan et al. 1984); molecular clouds in the Galaxy, e.g. the Orion Molecular Cloud (Morris et al. 1977) and the Sgr B2 cloud (de Vicente et al. 2000); stellar atmospheres, e.g. Henkel et al. (1985); and also in a few external galaxies (see below). As it has an even higher dipole moment than HCN ($\mu = 3.724$ D (Wernli et al. 2007)), it should be able to trace even denser gas than HCN.

HC_3N might, together with HCN among others, have been one of the first molecules created in the "primordial soup" of abiogenesis (Orgel 2002), thus being a so called "life molecule". When discovered in open space, it is naturally not very likely to be a predecessor of life. However, HC_3N (and other "life molecules") in a cloud with massive star formation could suggest that some life molecules might be formed even before planets.

In the Galaxy, HC_3N is associated with warm, dense, shielded gas around young stars or star-forming regions, and is easily dissociated by UV radiation and reactions with C^+ ions (Meier & Turner 2005). It will form either C_2H or C_3N when being photo-dissociated (Cherchneff et al. 1993), and C_3H^+ or C_4N^+ when reacting with C^+ (Bohme & Raksit 1985). The reactions destroying HC_3N are:

$$\mathrm{HC_3N} + h\nu \longrightarrow \mathrm{C_2H} + \mathrm{CN}, \tag{3.1}$$

$$\mathrm{HC_3N} + h\nu \longrightarrow \mathrm{C_3N} + \mathrm{H}, \tag{3.2}$$

$$\mathrm{HC_3N} + \mathrm{C^+} \longrightarrow \mathrm{C_3H^+} + \mathrm{CN}, \tag{3.3}$$

$$\mathrm{HC_3N} + \mathrm{C^+} \longrightarrow \mathrm{C_4N^+} + \mathrm{H}. \tag{3.4}$$

In Irvine et al. (1987), the relative abundances of several molecules in the core and ridge of the Orion molecular cloud can be found. This can be used as a pointer of how common these molecules are in dense and thin molecular regions. The relative HC_3N abundance lies around 10^{-9} of the H_2 abundance in the core (dense region), and 10^{-10} in the ridge (thin region). This is a relatively small difference between

dense and thin regions, as compared to e.g. HCN, with about 10^{-7} of the H_2 abundance in the core, and 10^{-9} in the ridge.

The possible dissociation processes for HC_3N will be further discussed in Costagliola & Aalto (in prep.).

3.4 C_2H_2 and C_2H

Acetylene, C_2H_2, is a colourless flammable gas. It exists on grains in the interstellar medium (ISM) (Chapman et al. 2009). After boiling off from the grains, there are at least two possible paths it might follow: If a high UV field is present (in a PDR, which can be read out as "photo-dissociation region" or "photon dominated region"), it will photo-dissociate into the ethynyl radical, C_2H (Meier & Turner 2005, Cherchneff et al. 1993, Heikkilä et al. 1999):

$$C_2H_2 + h\nu \longrightarrow C_2H + H. \tag{3.5}$$

If not in a PDR (no strong UV field present), but CN (the cyano radical) is present, it will instead form HC_3N (Meier & Turner 2005, Chapman et al. 2009, Fukuzawa & Osamura 1997):

$$C_2H_2 + CN \longrightarrow HC_3N + H. \tag{3.6}$$

Thus, it should be expected that in a region where grains with C_2H_2 first were present, the abundances of HC_3N and C_2H should help tell whether a strong UV field is present or not (at least if CN also is present).

In Irvine et al. (1987), it can be seen that C_2H, contrarily to HC_3N, is two orders of magnitude more abundant in the Orion ridge than in its hot core. Possibly, the hot core shields the HC_3N and C_2H_2 from photo-dissociating into C_2H. Some of the C_2H_2 instead reacts with the CN (although not very abundant) and forms even more HC_3N.

4 STARBURST GALAXIES AND ACTIVE GALAXIES

Most galaxies show an electromagnetic emission spectrum roughly similar to that of a black-body, normally peaking in the visible or near-IR region. This does not mean that the galaxy is a compact black-body, but that its spectrum is composed of the black-body spectra of the billions of stars as well as the interstellar gas and dust within the galaxy. In other words, the galaxy spectrum is the sum of the thermal emission originating from the components of the galaxy.

Some galaxies do not show this behaviour. Their electromagnetic spectra do not follow black-body curves, and they are normally peaking in other regions than the spectra of the normal galaxies, e.g. in the radio, far-IR or X-ray regions.

Many galaxies have strong sources of infrared radiation in their centres. This is probably caused by different effects in different galaxies (or, possibly, a combination of effects in some). One possibility is that the galaxy has an unusually high star formation rate – it is a starburst galaxy. Another possibility is that the galactic centre possesses a massive black hole onto which mass is accreted, generating enormous amounts of energy. This is called an Active Galactic Nucleus (AGN), and these galaxies are referred to as AGN galaxies, sometimes broken down to Seyferts (1 and 2), quasars, radio galaxies, etc. Many of these different classes of AGN galaxies are thought to be of the same kind, only observed from different directions, according to the unification theory for active galactic nuclei (Carroll & Ostlie 2007).

Most of these galactic centres are covered with dust (e.g. silicates) – starburst regions need large dust clouds to feed the star formation and AGNs are surrounded by accretion disks of dust. Since the source of the energy generation is obscured by the dust, it can often be hard to tell which galaxies are AGNs, and which are starbursts (SBs), as most of the characteristic radiation from the centres of these galaxies will be absorbed by the dust and re-emitted as infrared black-body radiation (heat).

The strong infrared radiation in some galaxies could also be a direct effect of a collision with another galaxy (e.g. Cox 1995); or perhaps be similar to a starburst, except the infrared radiation is powered by a population of older stars instead of newly formed stars (Thronson et al. 1990).

Note that both AGN galaxies and starburst galaxies can be defined as “active” galaxies, even though some texts will use “active galaxy” as a synonym for “AGN galaxy”.

Much is still unknown about these galaxies, and a lot of work has been done trying to separate them from each other (e.g. Aalto et al. 2007a, Aalto 2008, Albrecht et al. 2007, Cid Fernandes et al. 2001, Farrah et al. 2003, Krips et al. 2008, Sanders & Ishida 2004).

For an extensive discussion of the properties of starburst galaxies and galaxies with active galactic nuclei (AGNs), refer to e.g. Carroll & Ostlie (2007), Olsson (2009) or Pérez-Beaupuits (2006). In this section, a brief summary of the most

important properties of these galaxies, mainly based on these three references, will be given.

4.1 Starburst galaxies

Starburst galaxies are galaxies with an enormous rate of star formation, producing between 10 and 300 solar masses of stars per year (Carroll & Ostlie 2007), mostly going on in the central kpc of the galaxy (ordinary galaxies only produce stars in the order of 1 solar mass per year (Carroll & Ostlie 2007)). Generally, a starburst galaxy will maintain a high rate of star formation for 10^8 - 10^9 years (Carroll & Ostlie 2007).

The intensive luminosity of starburst galaxies generates extra radiation, generally emitted in the UV spectrum (due to the black-body temperatures of the stars). However, the star forming regions are deeply enshrouded by dust and gas clouds (star formation can only occur in dense clouds that provide material for the forming stars), which absorb the UV radiation. The dust is heated, and re-radiates the absorbed energy through IR radiation. Thus, a starburst galaxy will have a major proportion of its energy emitted in the infrared spectrum, although some will also be emitted in the UV or visible.

It is widely accepted that most starburst galaxies generally are or have been in a state of interacting or merging with another galaxy, why it is believed that galaxy interactions might trigger starbursts. This theory has been supported by simulations (Martig & Bournaud 2008). It has been claimed that all merging galaxy pairs will result in a starburst galaxy, but a survey performed by Bergvall et al. (2003) shows that interaction or merging might be a necessary criterion for creating a starburst galaxy, but definitely not a sufficient criterion. Only a modest increase of star formation was found in most of the studied interacting galaxies.

4.2 Active Galactic Nuclei

There are many different kinds of active galaxies - Seyfert 1s and 2s, LINERs, radio galaxies, quasars, blazars, etc. The Unified Model of Active Galactic Nuclei (AGNs) tries to unify all these to be the same sort of galaxy, just seen from different angles – e.g. blazars are observed when the accretion disk is face-on to the observer, Seyfert 1s when the disk is somewhat tilted away from the observer, and Seyfert 2s when it is observed edge-on. I will not attempt to explain the properties of the different types (or observation angles), as thorough descriptions can be found in most introductory textbooks on extragalactic astrophysics, such as Carroll & Ostlie (2007). A basic explanation of the properties of the energy source in the core of an AGN galaxy is, however, in its place.

An AGN is believed to be powered by a supermassive black hole, with a typical mass of about $10^8 M_\odot$[1] (Carroll & Ostlie 2007). This gives rise to the most efficient energy generation that is known to be possible: material in a gravitational potential that is accreted onto a compact object. Energy generation by matter falling straight

[1]The subscript $\odot$ denotes "solar", thus $M_\odot$ = "solar mass", $L_\odot$ = "solar luminosity", etc.

onto a black hole will however be very inefficient, since there is no surface onto which the matter will make impact as it falls into the black hole – as the matter approaches the event horizon, it will slow down and finally disappear beyond this limit. If matter instead spirals into the black hole in an accretion disk, collisions and viscous forces will generate heat and radiation corresponding to at most 42.3% of the matter's rest mass (Carroll & Ostlie 2007). This can be compared to nuclear reactions, which at most convert a little less than one percent of the reactants' masses into energy. Note that no matter is annihilated in the process, it is only the gravitational potential energy of the matter that is converted first to kinetic energy (when the matter falls onto the black hole), and then radiation (when the matter makes impact).

The energy generated in the accretion disk generally peaks in the UV spectrum (Carroll & Ostlie 2007), causing a big "blue bump" in many AGN galaxy spectra, but if the disk is obscured by gas and dust (which does not need to imply a star-forming region), this radiation will be absorbed by the dust, and re-radiated in the infrared spectrum, thus making it hard to distinguish the AGN galaxy from a starburst galaxy.

Some AGN galaxies also have strong radio and X-ray features, and often much of the radio frequencies originate from "radio lobes" protruding out from the black hole through jets of charged particles. These lobes can sometimes extend longer than the galaxy itself, to several tens of kpcs outside the AGN, but can also be rather compact. However, all AGN galaxies do not have radio lobes, and even if a certain galaxy does, depending on the viewing angle, they can sometimes be difficult to detect.

As the starburst galaxies, many of the AGN galaxies have companion galaxies with which they interact. For instance, these companions might supply the central black hole with fuel to power the AGN (Carroll & Ostlie 2007).

4.3 Composites of Starbursts and AGNs

Some galaxies seem to be hosting an AGN at the same time as they are experiencing a starburst period. These galaxies show the characteristic properties of both SBs and AGNs. Cid Fernandes et al. (2001) claims that these galaxies are more luminous than normal AGN galaxies.

It has been suggested that AGN galaxies and starburst galaxies are on different stages of an ongoing evolution. In this case, the composite galaxies might be in a transition phase between AGN and starburst. If this is true, it is still not certain which comes first, AGN or starburst. Cid Fernandes et al. (2001) claim that they finally will end up as Seyfert 2 galaxies (AGN galaxies), possibly with a faint starburst still going on, but weak compared to the AGN.

Calculations by Norman & Scoville (1988) show that a black hole can be formed in the centre of a starburst galaxy as a direct result of the starburst, as the mass loss from the evolving upper main-sequence stars in the starburst start to form a compact central mass. Contrarily, van Breugel et al. (1985) claim that some starbursts are triggered by radio jets from AGNs.

Some obscured Seyfert galaxies might also mimic some starburst properties – or the other way around – thus appearing as composites.

4.4 How to tell them apart

If a galaxy is very luminous in the IR spectrum ($L_{\mathrm{FIR}} \gtrsim 10^9 - 10^{10} L_\odot$), this indicates that most of its radiation is emitted by gas and/or dust heated by some other strong energy source, such as a starburst or an AGN. In many cases, it is hard to tell these two possibilities apart. However, some signs may clearly vindicate an AGN classification, such as hard X-ray emission and the existence of a broad line region (BLR) (Laor 2004).

All AGN galaxies do not show BLRs, and in galaxies with deeply obscured cores a BLR might not be detectable. The radio core might also be covered by thermal free-free emission, and X-ray emission might be absorbed if the source is Compton thick ($N(\mathrm{H_2}) > 10^{24}$ cm^{-2}). In such cases, there is no fool-proof method for telling an AGN galaxy apart from a starburst galaxy. Instead, many different criteria for the two types are tested individually. For nearby galaxies, the morphology of the region emitting the radio continuum might be studied. For starburst galaxies, the highest intensity peaks are expected to come from supernova remnants (SNRs), but in an AGN galaxy a compact core with perpendicular jets will be visible.

For more distant objects, the brightness temperature of the radio emission can be used. AGN galaxies are expected to have extremely high temperatures in the accretion disks, and the radio brightness temperatures could be of the order or 10^7 K, while starburst galaxies should have temperatures around $10^4 - 10^5$ K.

One of the most used methods for classifying AGN galaxies and starburst galaxies is described in Veilleux & Osterbrock (1987), and is a method based on atomic spectral lines in the optical spectrum (more specifically the Hα, Hβ, N II, O I, O III and S II lines).

Perhaps we could in the future use certain molecular tracers to investigate whether a galaxy with obscured core should belong to the starburst or AGN galaxies. Today's knowledge about molecular lines and line ratios used for telling starbursts apart from AGNs is both limited and disputed. I have thus chosen not to present any or all of these different theories, as they probably are subject to change in the near future.

4.5 LIRGs and ULIRGs

A Luminous Infrared Galaxy (LIRG) is a galaxy that emits more than $10^{11} L_\odot$ in the far infrared (FIR) spectrum. An Ultra-luminous Infrared Galaxy (ULIRG) emits more than $10^{12} L_\odot$ in the FIR spectrum. This does not tell whether the strong IR luminosity is powered by an AGN or a starburst, and in some articles, (U)LIRG is seen as a third possible classification of an active galaxy, along with starburst and AGN. Mostly, such classifications just show that the source for the strong IR radiation in that particular galaxy is unknown.

The majority of (U)LIRGs, like starbursts and AGN galaxies, merging galaxies or galaxies with tidal interactions with another galaxy (Sanders & Ishida 2004).

The difficulty in classifying the (U)LIRGs partly lies in most of them having extremely obscured central regions. They often show near-IR colours similar to those of Seyfert galaxies, but have no hard X-ray radiation, thus being more similar

to starbursts. Nevertheless, an AGN might still be present, although deeply buried in dust. See e.g. Genzel et al. (2000) for an extensive discussion.

This information justifies the classification of these galaxies as (U)LIRGs – it is certainly not a description of the energy source in these galaxies, however, as the individual galaxies seem to have much in common, (U)LIRG might be useful at least as an interim classification, until more knowledge about these objects is gained.

5 OBSERVATIONS AND SAMPLE

In this chapter, the selection of the sample of investigated galaxies and the properties of the galaxies in the sample are discussed. There are also a few words about the methods of observations, especially the importance of knowing the difference between the temperature scales used in radio astronomy.

5.1 Earlier observations of HC_3N in external galaxies

Some HC_3N measurements in other galaxies have been performed earlier, the first being Henkel et al. (1988), who detected HC_3N in IC 342 and M82, two nearby starburst galaxies.

Since then, detections of HC_3N in five other galaxies have been published: NGC 253 (Mauersberger et al. 1990), Arp 220 and NGC 1808 (Aalto et al. 2002), NGC 4945 (Wang et al. 2004) and NGC 4418 (Aalto et al. 2007a). The detections of HC_3N in six more galaxies will be reported in this text, and upper limits on the HC_3N line have been estimated for another 14 galaxies. These new measurements were carried out by S. Aalto, F. Costagliola, R. Monje, S. Muller and J.-P. Pérez-Beaupuits in 2001, 2006 and 2007. These measurements were performed with the telescopes SEST 15 m (2001), IRAM 30 m (2006-2007), OSO 20 m (2001) and JCMT 15 m (2007).

The HC_3N molecule has very many known rotational transitions. This is because its 1-0 transition has a very low frequency, which in turn depends on this frequency being inversely proportional to the moment of inertia of the molecule – as HC_3N is a long, straight molecule, its moment of inertia is quite high.

Luckily, most of the HC_3N line measurements found in the literature are of the 10-9 transition, making it easier to compare the intensities in the different galaxies. There are several reasons for the choice of the 10-9 line, one being its proximity to the HCN 1-0 and HNC 1-0 lines, which are tracers of dense gas, and good reference molecules which can be used to compare the HC_3N value with. Some of the HC_3N 10-9 lines have been measured in the same spectra as the HNC 1-0 lines, as the bandwidth of SEST could include both of them. Another reason to choose the 10-9 transition is that no other transitions expected in the sources lie so close that they risk blending with the HC_3N line (the separation between the HNC 1-0 and HC_3N 10-9 lines corresponds to a Doppler velocity of approximately 1000 km/s, and the line widths of the observed sources rarely exceed 500 km/s).

5.2 Observations in this work

The new measurements reported in this work were carried out with the IRAM 30 m, OSO 20 m, SEST 15 m and JCMT 15 m telescopes. In the survey, data from the literature using these telescopes, as well as the NRO 45 m, NRAO 12 m, CSO 10.4 m and FCRAO 14 m telescopes, and the OVRO array, are included. Whenever using data from the literature, the beam sizes and efficiencies given in the respective

articles have been used for calculations of line ratios. The parameters used for all new measurements reported in this work are given in Table 5.1.

All objects investigated (observed by us or found in the literature) are listed in Table 5.2, along with some important characteristics.

Detailed lists of the observers and dates for the observations reported in this work are found in Tables 5.3-5.5.

When performing the measurements, the absolute intensities of certain molecules in certain galaxies are not that interesting. To be able to tell whether the HC_3N is abundant or not, its intensity must be compared with the intensities of other, more common, molecules. The intensities are compared by calculating a *line ratio* between the two spectral line intensities. The method for this is described in Section 6.2

Note that some of the galaxies have so large angular distribution that the measured values might not represent a global value for the galaxy, but rather a value for a certain (central) region of the galaxy. If the different measurements for the same galaxy are taken in different parts of the galaxies, the line ratios might be corrupt. The exact positions of measurement are given in most of the references, and these have been compared. The largest difference in position between two measurements in the same galaxy is for IC 342, which has a $3''$ difference between the HCN measurement in Sorai et al. (2002) and the HNC and HC_3N measurements in Henkel et al. (1988). Investigating the HNC and HC_3N maps in Meier & Turner (2005), it turns out that the structures of molecular gas in the galaxy are so large that this difference in positions should not pose a big problem. For all other galaxies, the position difference is at most $1''$.

Another issue is that two molecules compared in a line ratio might not have the same spatial distribution, and thus a too narrow beam might exclude more flux from one molecule than from the other. The problem gets even greater if the two molecular lines are measured with two different beam sizes.

This is particularly a problem for the measurements of Circinus, IC 342, M82, Maffei 2, NGC 253, NGC 613, NGC 1365, NGC 1808 and NGC 2146, due to their large source sizes, but the problem is of course also dependent on the beam size used for each observation. The galaxies for which the observations have been performed with $\theta_{\mathrm{beam}} \lesssim \theta_{\mathrm{source}}$ are IC 342, M82, Maffei 2, NGC 253, and NGC 2146.

The size of the dense region is of importance when converting from measured temperature to brightness temperature (this is explained in Sections 5.3 and 6.2), and as a consequence of this also when computing the line ratios between two transitions in a galaxy. When available, the source size has been estimated from tables or maps showing the source size of the HCN emission, thus assuming that the HCN source size is of the same order as the source sizes of the other molecules used in the line ratio calculations (HNC and HC_3N). When an HCN source size has not been found, the source size of CO emission has been used instead, preferably the higher transitions, as these are better tracers of dense gas than CO 1-0, which traces much thinner molecular gas, thus giving a too high value on the source size. The source sizes used in this work are shown in Table 5.2. Unless no transition is stated, HCN 1-0 should be assumed.

Note that for some of the galaxies no reliable value on the source size has been found. This might still not be a problem when calculating the line ratios, and this

Table 5.1. Observational parameters

Transition	ν [GHz][a]	HPBW [″][b]	η_{mb}[b]
IRAM:			
HC_3N 10-9	90.979	28	0.80
HC_3N 16-15	145.561	17	0.67
HC_3N 25-24	227.419	10.5	0.63
HC_3N 28-27	254.699	9	0.59
HCN 1-0	88.632	28	0.80
HCN 3-2	265.886	9	0.57
HNC 1-0	90.664	28	0.80
HNC 3-2	271.981	9	0.57
OSO:			
HC_3N 12-11	109.174	36	0.52
HC_3N 10-9	90.979	42	0.59
SEST:			
HC_3N 10-9	90.979	55	0.75
HCN 1-0	88.632	57	0.75
HNC 1-0	90.664	55	0.75
JCMT:			
HC_3N 38-37	345.609	15	0.64
HC_3N 39-38	354.697	14	0.63

[a] From NIST Recommended Rest Frequencies (Frank J. Lovas).

[b] The half-power beamwidths and main beam efficiencies are copied from the respective telescope web pages.

will be further discussed in Section 6.2.1.

The sample of galaxies observed by us has been chosen to have a large probability of finding HC_3N – it is by no means intended to be an unbiased sample of some random galaxies, and thus the detection rate should definitely not reflect the amount of HC_3N-luminous galaxies in the universe. The same is most likely true for the galaxies found in the literature. Another important selection effect for the objects from the literature is that detections are much more likely to be reported than non-detections, which also leads to a biased sample.

To increase the chance of detecting HC_3N, almost all of the galaxies that were chosen to be part of the sample have earlier detections of HCN, which means that they should have large amounts of dense gas, increasing the possibility of finding HC_3N. As the goal of the study is to investigate if HC_3N can trace the source of the activity in active galaxies, the sample consists only of active galaxies – starburst galaxies and AGN galaxies (the source of the activity is although disputed or unknown in many of the galaxies in the sample).

Table 5.2. Investigated objects

Galaxy	Type[a]	cz[b] [km s^{-1}]	D[c] [Mpc]	$\log L_{\rm FIR}$[d] [$L_\odot$]	$\theta_{\rm HCN}$[e] [″]
Arp 220	ULIRG, Obsc., SB?	5450	78.1	12.15	2[1]
Circinus	AGN (cp?)	434[f]	3.13	...	21 (CO 3-2)[2]
IC 342	SB	31	4.00	10.01	20[3]
IC 694[g]	SB	3159	58.2	11.74[h]	5[4]
IC 860	Obsc.	3887	59.1[d]	11.14	*
I17208[i]	ULIRG, Obsc. (SB?)	12852	178	12.35	0.67[5]
M82	SB	187	5.68	10.61	> 30[1]
Maffei 2	SB	-17[f]	3.34	...	20×7[6]
NGC 34	SB	5931	79.8	11.34	*
NGC 253	SB	261	3.22	10.29	18×8[7]
NGC 613	cp	1475	18.6	10.22	40 (CO 1-0)[8]
NGC 1056	AGN	1545	22.7	9.79	-
NGC 1068	cp	1005	15.3	10.89	4.5[1]
NGC 1365	cp	1636	19.9	10.86	34 (CO 2-1)[9]
NGC 1377	Obsc., AGN?	1792	22.5	9.95	-
NGC 1614	SB	4746	63.4	11.43	12 (CO 2-1)[10]
NGC 1808	SB (cp?)	1000	11.2	10.55	18 (CO 2-1)[10]
NGC 2146	SB	885	16.9	10.93	20[1]
NGC 2623	SB	5538	76.9	11.48	1.8[11]
NGC 3079	SB? AGN?	1142	19.7	10.65	13×5 (CO 1-0)[12]
NGC 3256	SB	2781	36.5	11.43	9 (CO 2-1)[10]
NGC 3690[g]	SB	3159	46.9	11.74[h]	1.56[5]
NGC 4418	Obsc., AGN?	2104	32.6	11.00	5 (CO 1-0)[13]
NGC 4945	SB (cp?)	560	4.85	10.41	15 (CO 3-2)[2]
NGC 5135	cp	4114	56.0	11.06	15×5 (CO 1-0)[14]
NGC 6946	SB	53	5.64	10.01	10[1]
NGC 7130	cp	4824	65.4	11.23	10 (CO 1-0)[10]
UGC 5101	(U)LIRG, cp	11785	165	11.87	3.50 (CO 1-0)[5]

[a] See discussion in Section 5.2.1 for references. SB = Starburst, AGN = Active Galactic Nucleus, cp = composite of SB and AGN, Obsc. = obscured, ULIRG = Ultra-luminous Infrared galaxy.

[b] Heliocentric radial velocity of source, from Sanders et al. (2003).

[c] Distance to source, corrected for Virgo infall only, from NED (2009).

[d] From Sanders et al. (2003).

[e] Source sizes, given for HCN 1-0 line if not specified otherwise, taken from: (1) table in Krips et al. (2008), (2) table in Curran et al. (2001a), (3) HCN map in Meier & Turner (2005), (4) HCN map in Aalto et al. (1997), (5) table in Graciá-Carpio et al. (2008), (6) HCN map in Nguyen-Rieu et al. (1994), (7) HCN map in Knudsen et al. (2007), (8) CO 1-0 map in Bajaja et al. (1995), (9) CO 2-1 source size in Curran et al. (2001b), (10) table in Aalto et al. (1995), (11) table in Bryant & Scoville (1999) (12) CO 1-0 map in Koda et al. (2002), (13) CO 1-0 map in Dale et al. (2005), (14) CO 1-0 map in Regan et al. (1999).

For galaxies with an asterisk (*), no value has been found, but $D \gtrsim 50$ Mpc, allowing the point-like approximation ($\theta_{\rm HCN} = 0$) with an error $\lesssim 5\%$ (see Section 6.2.1). For galaxies marked with a dash (-), no value has been found, and $D < 50$ Mpc.

[f] From NED (2009).

[g] IC 694 and NGC 3690 are also known as the merger Arp 299.

[h] This is the FIR luminosity of IC 694 and NGC 3690 together.

[i] Short for IRAS 17208-0014.

Table 5.3. Observers, positions, and observation dates for HC_3N data reported in this work (for the observations cited from the literature, refer to the respective articles referred to in Table 6.1).

Galaxy	R.A. (J2000.0)	Decl. (J2000.0)	Line	Observer[a]	Telescope	Date
Arp 220	15 34 57.1	+23 30 11.3	10-9	SA	OSO 20 m	2001-11-11
Arp 220	15 34 57.1	+23 30 11.3	12-11	SA	OSO 20 m	2001-11-09
IC 694	11 28 33.6	+58 33 46.0	12-11	SA	OSO 20 m	2001-11-10
IC 860	13 15 03.5	+24 37 08.0	28-27	FC	IRAM 30 m	2007-12-16
I17208	17 23 21.9	−00 17 00.9	10-9	FC	IRAM 30 m	2007-12-16
Maffei 2	02 41 55.1	+59 36 15.0	12-11	SM	IRAM 30 m	2007-08
NGC 1056	02 42 48.3	+28 34 27.1	16-15	RM, JP	IRAM 30 m	2006-06-30
NGC 1377	03 36 39.1	−20 54 08.0	16-15	FC	IRAM 30 m	2007-12-13
NGC 1377	03 36 39.1	−20 54 08.0	25-24	FC	IRAM 30 m	2007-12-13
NGC 2146	06 18 37.8	+78 21 22.9	10-9	SA	OSO 20 m	2001-11-08
NGC 2146	06 18 37.8	+78 21 22.9	12-11	SA	OSO 20 m	2001-11-08
NGC 2623	08 38 24.1	+25 45 17.2	12-11	SA	OSO 20 m	2001-11-12
NGC 3079	10 01 57.8	+55 40 47.1	10-9	SA	IRAM 30 m	2006-05-14
NGC 3079	10 01 57.8	+55 40 47.1	16-15	SA	IRAM 30 m	2006-05-14
NGC 3079	10 01 57.8	+55 40 47.1	25-24	SA	IRAM 30 m	2006-05-14
NGC 3690	11 28 31.0	+58 33 40.0	12-11	SA	OSO 20 m	2001-11-09
NGC 4418	12 26 54.8	−00 52 42.0	38-37	RM	JCMT 15 m	2007-05-01
NGC 4418	12 26 54.8	−00 52 42.0	39-38	RM	JCMT 15 m	2007-05-04
NGC 6946	20 34 52.3	+60 09 14.0	12-11	SM	IRAM 30 m	2007-08
UGC 5101	09 35 51.6	+61 21 11.7	10-9	FC	IRAM 30 m	2007-12-13

[a] SA = Susanne Aalto, FC = Francesco Costagliola, SM = Sebastien Muller, RM = Raquel Monje, JP = Juan-Pablo Pérez-Beaupuits.

Table 5.4. Observers, positions, and observation dates for HCN 1-0 data reported in this work (for the observations cited from the literature, refer to the respective articles referred to in Table 6.2).

Galaxy	R.A. (J2000.0)	Decl. (J2000.0)	Observer[a]	Telescope	Date
NGC 613	01 36 36.7	−29 09 50.4	SA	SEST 15 m	2001-02-11
NGC 1377	03 36 39.1	−20 54 08.0	FC	IRAM 30 m	2007-12-13
NGC 4418	12 26 54.6	−00 52 39.6	RM	IRAM 30 m	2008-07-19

[a] SA = Susanne Aalto, FC = Francesco Costagliola, RM = Raquel Monje.

Table 5.5. Observers, positions, and observation dates for HNC 1-0 data reported in this work (for the observations cited from the literature, refer to the respective articles referred to in Table 6.3). Note that some of the HC_3N 10-9 data reported by us come from these HNC 1-0 spectra, as both lines will fit inside the SEST bandwidth.

Galaxy	R.A. (J2000.0)	Decl. (J2000.0)	Observer[a]	Telescope	Date
Circinus	14 10 34.3	−64 52 12.5	SA	SEST 15 m	2001-01-14
IC 860	13 15 03.5	+24 37 08.0	FC	IRAM 30 m	2007-12-16
I17208	17 23 21.9	−00 17 00.9	RM, JP	IRAM 30 m	2006-06-28
NGC 34	00 11 06.5	−12 06 26.6	SA	SEST 15 m	2001-01-14
NGC 613	01 36 36.7	−29 09 50.4	SA	SEST 15 m	2001-02-13
NGC 1056	02 42 48.3	+28 34 27.1	RM, JP	IRAM 30 m	2006-06-30
NGC 1377	03 36 39.1	–20 54 08.0	FC	IRAM	2007-12-13
NGC 1614	04 36 24.2	–08 28 40.3	SA	SEST	2001-02-13
NGC 4945	13 05 27.0	−49 28 04.5	SA	SEST 15 m	2001-01-15
NGC 5135	13 25 44.0	−29 50 02.2	SA	SEST 15 m	2001-01-13
UGC 5101	09 35 51.6	+61 21 11.7	FC	IRAM 30 m	2007-12-13

[a] SA = Susanne Aalto, FC = Francesco Costagliola, RM = Raquel Monje, JP = Juan-Pablo Pérez-Beaupuits.

5.2.1 Galaxy classification

When analysing the data, trying to draw conclusions whether an abundance of this-or-that molecule could indicate that a galaxy can be put into a certain category, it would of course be beneficial to know the categorisation of most of the galaxies in the sample on beforehand. Unfortunately, it is still debated what signs should make an active galaxy identified as an AGN rather than a starburst, or the other way around – this work is intended to facilitate this classification. However, our theory must be compared with what is the general belief of the scientific community. Below I give brief descriptions of the galaxies in our sample including their classifications. A summary of the classifications below is found in Table 5.2.

Any given distances or other specific values in the following sections are taken from Sanders et al. (2003) if no other reference is specified. For a lengthier discussion of each of the galaxies, refer to the Notes section at NED (2009). The classifications given directly on the galaxies' main pages on NED (2009) should, however, not be trusted, as they often disagree with the majority of the articles dealing with the respective galaxy (see Appendix B).

Arp 220

Arp 220 is a galaxy so special that loads of articles have been written about this galaxy alone. It is one of the most luminous galaxy in the IRAS sample, with a $L_{\mathrm{FIR}} \sim 10^{12} L_{\odot}$ (Thomas et al. 2004), thus placing it in the ULIRG category. It is a merging galaxy, and at a distance of about 80 Mpc, the two galaxy cores are

separated by less than an arcsecond on the sky.

As it suffers from a high degree of obscuration (Surace et al. 2000), it is very hard to determine if its activity is powered by an AGN or a starburst. E.g. Farrah et al. (2003), however claim that it is best interpreted as a starburst galaxy.

The galaxy contains an OH-megamaser (Baan & Haschick 1984), which was one of the first of its kind to be discovered.

Circinus

The Circinus galaxy is a very nearby galaxy (3 Mpc). It is definitely an AGN galaxy, more exactly a Seyfert 2, but could also contain a starburst almost as strong as the AGN luminosity, although the very centre of the galaxy is dominated by the AGN (Sosa-Brito et al. 2001). It has H_2O-megamaser activity (Sosa-Brito et al. 2001). Even though it is the most nearby galaxy in the sample, its source size is small enough not to exceed the beam size. This is due both to the galaxy being relatively small, and that all measurements on the galaxy were made with the SEST telescope, which has the largest beam of the used telescopes.

IC 342

IC 342 is a barred spiral galaxy (Sheth et al. 2002) with a ring-shaped young starburst region surrounding the galaxy centre (Förster Schreiber et al. 2004). As the galaxy subtends a large angle on the sky, high-resolved mappings of molecules in the galaxy are relatively easy to perform (Meier & Turner 2005).

IC 694

IC 694 is merging together with the galaxy NGC 3690 (see below). The system of the two galaxies is often referred to as Arp 299. It is most probably a starburst galaxy (Kinney et al. 1993).

IC 860

IC 860 is considered to be a relatively "normal" object as compared to most of the other sources in this list, and is thus one of the less well-studied sources in the sample. It has a deeply obscured nucleus (Lahuis et al. 2007), and it is thus hard to tell if its IR luminosity is powered by an AGN or a starburst. It contains an OH megamaser (Zhi-yao 2003).

IRAS 17208-0014

I17208 is one of the most luminous sources in the IRAS catalogue. It is also the most distant source in this sample (178 Mpc). The galactic nucleus is deeply obscured (Zink et al. 2000), but Farrah et al. (2003) claim that it is more likely to be powered by a starburst than an AGN. It contains an OH megamaser (Zink et al. 2000).

M82

M82 is a very nearby (6 Mpc) starburst galaxy. Its starburst has probably been triggered by interaction with its companion galaxy M81 (Marcum et al. 2001).

Maffei 2

Maffei 2 is one of the most nearby galaxies in the sample (3 Mpc), but considering its proximity, it hasn't been studied to a particularly high extent. It is a relatively small galaxy, and has a relatively weak IR luminosity, but is considered to be a starburst galaxy (Mason & Wilson 2004).

NGC 34

NGC 34 is a merger galaxy in the latter parts of the merging process. It has earlier been classified as a Seyfert galaxy, but it is now generally agreed that it is more likely to be a starburst galaxy (Thean et al. 2000).

NGC 253

NGC 253 is a very nearby (3 Mpc) starburst galaxy, but as it has no close companions, the trigger of the starburst activity is unknown (Strickland et al. 2004).

NGC 613

NGC 613 is sometimes described as a Seyfert galaxy (Jungwiert et al. 1997), and sometimes as a starburst galaxy (Spoon et al. 2002). According to Veron et al. (1997), it is has a composite spectrum, showing both Seyfert and H II region features.

NGC 1056

NGC 1056, sometimes referred to as Mrk 1183, is not one of the more well-studied galaxies in the sample, but is considered being a Seyfert galaxy (Thean et al. 2000).

NGC 1068

NGC 1068 is the most nearby Seyfert 2 galaxy, but does also contain a circumnuclear starburst (Papovich et al. 2003), thus making it a composite galaxy. It contains a strong H_2O megamaser (Kartje et al. 1999).

NGC 1365

Spoon et al. (2002) and many others see this galaxy as a Seyfert galaxy, but Reunanen et al. (2003) claims that it also is undergoing major starburst activity in a ring around its nucleus. Thus, this galaxy is probably best seen as a composite galaxy.

NGC 1377

At first glance, this galaxy seems to be quite normal, but since its core is deeply obscured, it might hide an AGN or a starburst in its core. Imanishi (2006b) considers it to be a deeply obscured AGN.

NGC 1614

NGC 1614 is a galaxy in the latter parts of a merging process (Hattori et al. 2004). Lancon et al. (1996) and Olsson (2009) claim it to be a starburst galaxy, which seems more accepted than the Seyfert 2 classification given by NED (2009).

NGC 1808

According to Lutz et al. (2004), NGC 1808 contains both a strong starburst and a weaker AGN. Few other articles mention the AGN, although both NED (2009) and Spoon et al. (2002) classify it as a Seyfert 2. Jungwiert et al. (1997) confirm the starburst classification.

NGC 2146

NGC 2146 is probably a post-merger undergoing starburst activity (Marcum et al. 2001). It has a very peculiar shape, its spiral arms are warped out of the galactic plane, probably the result of the earlier merging process.

NGC 2623

The emission of NGC 2623 is dominated by a starburst, and the object is a nearly completed merger of three galaxies (Smith et al. 1996).

NGC 3079

Strickland et al. (2004) claim NGC 3079 to be a LINER galaxy, with a disk-wide starburst activity, probably combined with a weaker AGN. Sosa-Brito et al. (2001) classify it as a Seyfert 2, probably with a strong nuclear starburst and maybe an AGN. It is the host of an H_2O megamaser.

NGC 3256

NGC 3256 has a very large starburst region (4 kpc). This LIRG shows tidal tails, probably a trace of a merging. (Kinney et al. 1993)

NGC 3690

NGC 3690 is merging together with IC 694 (see above). It has starburst activity, probably caused by the merging process (Conselice et al. 2000).

NGC 4418

NGC 4418 is a very unusual object on many accounts. The nucleus is heavily obscured by silicate dust, maybe hosting an early AGN (Thomas et al. 2002, Wynn-Williams & Becklin 1993). It has a very rich chemistry (Costagliola & Aalto in prep.). It is the host of a quite faint OH megamaser (Malhotra et al. 1996).

NGC 4945

NGC 4945 is widely accepted to be a starburst galaxy, but could also harbour an AGN (Sosa-Brito et al. 2001). It hosts an H_2O megamaser (Moorwood & Glass 1984). As it is very nearby (5 Mpc), its chemistry is quite well-known (see e.g. Wang et al. (2004)).

NGC 5135

This galaxy has been described both as a Seyfert and a starburst galaxy (Cid Fernandes et al. 1998). Its mixed starburst and Seyfert features may suggest that it might be undergoing a transition from starburst to Seyfert (Thuan 1984).

NGC 6946

NGC 6946 hosts a minor starburst at its centre (Alton et al. 1998). It seems to be a quite undisturbed spiral galaxy.

NGC 7130

NGC 7130 is similar to NGC 5135, having a Seyfert nucleus surrounded by a starburst region (Cid Fernandes et al. 1998).

UGC 5101

The second most distant object in our sample, UGC 5101 (165 Mpc), is a LIRG. It has been classified both as AGN and starburst, and is claimed to be a composite by Farrah et al. (2003). It contains an OH megamaser (Zhi-yao 2003) and one of the strongest H_2O megamasers ever detected (Zhang et al. 2006).

5.3 Temperature scales

When comparing radio astronomical data from different sources in the literature, it is very important to pay attention to the different temperature scales used by radio astronomers. A lengthy discussion about these different temperature scales can be found in Rohlfs & Wilson (2004). However, a short explanation is in its place.

First, there is the brightness temperature, T_B, of the source. This is what radio astronomers actually want to measure. This should not be confused with the physical temperature T_phys of the source, as the brightness temperature more precisely is the temperature of a black body which will give the same spectral radiance (power per unit area per unit frequency interval per unit solid angle) as the source itself. In other

words, if the observed source can be approximated with a black body, its brightness temperature will be approximately equal to its physical temperature. For spectral lines, which obviously not are black body curves, the brightness temperature will not be directly related to the physical temperature, but rather to the excitation temperature $T_{\rm ex}$. This might in turn be equal to the physical temperature, but only if the system is in local thermal equilibrium (LTE).

The brightness temperature is rarely used in the literature. Instead, two antenna dependent temperature scales are seen more frequently, the main beam brightness temperature $T_{\rm mb}$ and the corrected antenna temperature $T_{\rm A}^*$.

The main beam brightness temperature is dependent on the size of the antenna beam, and is related to the brightness temperature by

$$T_{\rm mb} = T_{\rm B} \frac{\theta_{\rm s}^2}{\theta_{\rm s}^2 + \theta_{\rm b}^2}, \tag{5.1}$$

where $\theta_{\rm s}$ is the source size of the measured object and $\theta_{\rm b}$ (or $\theta_{\rm mb}$) is the size of the beam (both usually given in arcseconds). $T_{\rm mb}$ thus approaches $T_{\rm B}$ for sources much larger than the beam.

The corrected antenna temperature scale, $T_{\rm A}^*$, is used for the new data presented in this work (note that some of the data from the literature is given in $T_{\rm mb}$ scale). It is sometimes called forward beam brightness temperature, and is related to the antenna temperature of the source outside the earth's atmosphere $T_{\rm A}'$ by

$$T_{\rm A}^* = \frac{T_{\rm A}'}{F_{\rm eff}}, \tag{5.2}$$

where $F_{\rm eff}$ is the forward efficiency of the antenna. Finally, $T_{\rm A}^*$ can also be related to $T_{\rm mb}$ using the main beam efficiency $\eta_{\rm mb}$:

$$T_{\rm mb} = \frac{T_{\rm A}^*}{\eta_{\rm mb}}. \tag{5.3}$$

6 RESULTS

All new HC_3N, HCN and HNC spectra reported in this work are displayed in Appendix C. The measured values of these can be found in Tables 6.1-6.3. Additional data from the literature not measured in this work are also included in the tables.

Note that some measurements on HC_3N 10-9 and HNC 1-0 performed with SEST will include both these lines in the same spectrum, due to the large bandwidth. The spectra are labelled according to the central peak. The frequency difference between the two peaks is 315 MHz, as can be seen in Table 5.1. This gives a velocity difference of about 1000 km/s.

Some of the more nearby galaxies have angular distributions equal to or larger than the beam size. These measurements will not reflect a global value of the molecular abundances, but rather focus on certain (central) regions. These local measurements are thus needed to be discussed separately from the other, global, values. This is particularly the case for the measurements on IC 342, M82, Maffei 2 and NGC 253, and is further discussed in Chapter 7.

6.1 New detections

This is not only the first text to put together a survey of all extragalactic HC_3N measurements, but it also reports the first HC_3N detections in six galaxies: Circinus, IC 860, IRAS 17208-0014 (the most distant HC_3N detection yet reported), Maffei 2, NGC 1068 and NGC 3079. The number of extragalactic sources where HC_3N has been detected is thus almost doubled.

Three of the HNC detections are also made in sources without earlier HNC detections: Circinus, IC 860 and IRAS 17208-0014.

Finally, the first detection of HCN in NGC 613 is also reported.

6.2 Line ratios

When comparing the spectral lines between two different galaxies, we cannot just compare the intensity values, as such a comparison would not compensate for the galaxies being of different sizes, on different distances, and of different level of obscuration, as well as the measurements being made with different telescopes. It would also be interesting to not estimate just the amount of HC_3N as compared to the size of the galaxy, but instead as compared to the amount of other dense gas in the galaxy. Thus, the intensity ratio between HC_3N and another tracer of dense gas is sought. In this text, the comparison will be made both with HCN and HNC, primarily due to the fairly large amount of such data available, but other dense gas tracers could also be relevant for comparison.

When calculating line intensities, there are several factors to take into account. As the measurements might have been performed with different telescopes, the telescopes' beam efficiencies and beam sizes must be compensated for. More thorough derivations of the following formulae can be found in Rohlfs & Wilson (2004).

Table 6.1. Data from HC_3N measurements

Galaxy	Line	$I(HC_3N)$[a] [K km s^{-1}]	Δv [km s^{-1}]	Telescope	η_{mb}	θ_{mb} [$''$]	T scale[a]	Reference[b]
Arp 220	10-9	2.02 ± 0.3	340	OSO 20 m	0.59	44		(1)
Arp 220	10-9[c]	0.4 ± 0.15	350	SEST 15 m	0.75	55		(2)
Arp 220	12-11	0.96 ± 0.2	170	OSO 20 m	0.52	36		(1)
Circinus	10-9[d]	1.00 ± 0.2	290	SEST 15 m	0.75	55		(1)
IC 342	10-9	8.4 ± 1	30	OVRO array	...	5.9×5.1	T_{mb}	(3)
IC 342	10-9	2.6 ± 0.7	52	IRAM 30 m	0.8	25	T_R^*	(4)
IC 694	12-11	< 0.30	...	OSO 20 m	0.52	36		(1)
IC 860	28-27	0.54 ± 0.13	175	IRAM 30 m	0.59	9		(1)
I17208	10-9	0.33 ± 0.05	330	IRAM 30 m	0.80	28		(1)
M82	12-11	5.6 ± 0.6	155	IRAM 30 m	0.80	25	T_R^*	(4)
Maffei 2	12-11	1.84	230	IRAM 30 m	0.73	24		(1)
NGC 34	10-9[c]	< 0.45	...	SEST 15 m	0.75	55		(1)
NGC 253	10-9	5.8 ± 0.6	63	IRAM 30 m	...	26	T_{mb}	(5)
NGC 253	15-14	4.4 ± 0.4	77, 85	IRAM 30 m	...	19	T_{mb}	(6)
NGC 253	16-15	3.8	77[e], 85[e]	IRAM 30 m	...	17	T_{mb}	(6)
NGC 253	17-16	3.0 ± 0.2	72[e]	IRAM 30 m	...	16	T_{mb}	(6)
NGC 253	18-17	2.2 ± 0.7	73	IRAM 30 m	...	15	T_{mb}	(6)
NGC 253	19-18	4.6 ± 0.8	74	IRAM 30 m	...	14	T_{mb}	(6)
NGC 613	10-9[c]	< 0.26	...	SEST 15 m	0.75	55		(1)
NGC 1056	16-15	< 0.17	...	IRAM 30 m	0.67	17		(1)
NGC 1068	10-9[c]	0.35 ± 0.3	100	SEST 15 m	0.75	55		(1)
NGC 1365	10-9[c]	< 0.61	...	SEST 15 m	0.75	55		(1)
NGC 1377	16-15	< 0.28	...	IRAM 30 m	0.67	17		(1)
NGC 1377	25-24	< 0.26	...	IRAM 30 m	0.63	10.5		(1)
NGC 1614	10-9[c]	< 0.39	...	SEST 15 m	0.75	55		(1)
NGC 1808	10-9[c]	0.2 ± 0.1	250	SEST 15 m	0.75	57		(2)
NGC 2146	10-9	< 0.38	...	OSO 20 m	0.59	42		(1)
NGC 2146	12-11	< 0.38	...	OSO 20 m	0.52	36		(1)
NGC 2623	12-11	< 0.50	...	OSO 20 m	0.52	36		(1)
NGC 3079	10-9	0.60 ± 0.1	500	IRAM 30 m	0.80	28		(1)
NGC 3079	16-15	< 0.54	...	IRAM 30 m	0.80	28		(1)
NGC 3079	25-24	< 0.40	...	IRAM 30 m	0.80	28		(1)
NGC 3256	10-9[c]	< 0.12	...	SEST 15 m	0.75	55		(2)
NGC 3690	12-11	< 0.31	...	OSO 20 m	0.52	36		(1)
NGC 4418	10-9	0.8 ± 0.08	122	IRAM 30 m	0.77	27		(7)
NGC 4418	16-15[f]	1.7 ± 0.08	130	IRAM 30 m	0.70	17		(7)
NGC 4418	25-24	1.6 ± 0.2	140	IRAM 30 m	0.53	11		(7)
NGC 4418	38-37	1.5[g]	100	JCMT 15 m	0.64	15		(1)
NGC 4418	39-38	?[h]	...	JCMT 15 m	0.63	14		(1)
NGC 4945	9-8	2.16 ± 0.50	230	SEST 15 m	0.78	63	T_{mb}	(8)
NGC 4945	10-9	1.99 ± 0.21	290	SEST 15 m	0.75	55	T_{mb}	(8)
NGC 4945	11-10	2.92 ± 0.35	340	SEST 15 m	0.73	52	T_{mb}	(8)
NGC 4945	12-11	4.18 ± 0.38	340	SEST 15 m	0.71	49	T_{mb}	(8)
NGC 4945	15-14	2.13 ± 0.29	250	SEST 15 m	0.65	40	T_{mb}	(8)
NGC 4945	16-15[i]	5.02 ± 0.19	330	SEST 15 m	0.63	37	T_{mb}	(8)
NGC 4945	17-16	2.26 ± 0.55	280	SEST 15 m	0.61	33	T_{mb}	(8)
NGC 4945	24-23	< 0.60	...	SEST 15 m	0.48	23	T_{mb}	(8)
NGC 4945	25-24	< 0.60	...	SEST 15 m	0.46	22	T_{mb}	(8)
NGC 5135	10-9[c]	< 0.13	...	SEST 15 m	0.75	55		(1)
NGC 6946	12-11	< 0.28	...	IRAM 30 m	0.73	24		(1)
NGC 7130	10-9[c]	< 0.10	...	SEST 15 m	0.75	55		(2)
UGC 5101	10-9	< 0.12	...	IRAM 30 m	0.80	28		(1)

[a] Integrated intensities are in T_A^* if not stated differently. Upper limits are all 2σ.

[b] (1) This work, (2) Aalto et al. (2002), (3) Meier & Turner (2005), (4) Henkel et al. (1988), (5) Mauersberger et al. (1990), (6) Martín et al. (2006), (7) Aalto et al. (2007a), (8) Wang et al. (2004).

[c] Measured in HNC 1-0 spectrum.

[d] In the region with highest HC_3N value.

[e] Fixed when fitting Gaussian.

[f] Contaminated by para-H_2CO, estimated to 20%. The given value is only for the HC_3N component.

[g] Possible detection, but line is strongly contaminated by CO 3-2. The intensity value is thus a very uncertain approximation.

[h] Tentative detection, but line is strongly contaminated by HCN 4-3, and no value for the intensity has been established. See Costagliola & Aalto (in prep.).

[i] Contaminated by H_2CO.

Table 6.2. Data from HCN 1-0 measurements

Galaxy	I(HCN) 1-0[a] [K km s^{-1}]	Δv [km s^{-1}]	Telescope	$\eta_{\rm mb}$	$\theta_{\rm mb}$ [$''$]	T scale[a]	Reference[b]
Arp 220	9.7 ± 0.4	530	IRAM 30 m	0.82	29.5	$T_{\rm mb}$	(1)
Circinus	5.2 ± 0.8	300	SEST 15 m	0.75	57	$T_{\rm mb}$	(2)
IC 342	15.5 ± 0.9	...	NRO 45 m	0.54	19	$T_{\rm mb}$	(3)
IC 694	1.29 ± 0.09	...	IRAM 30 m	0.82	28		(4)
IC 860	...	...		...	...		N/A[c]
I17208	0.91 ± 0.19	...	NRAO 12 m	0.89	72	$T_{\rm R}^*$	(5)
I17208	2.19 ± 0.16	...	IRAM 30 m	0.82	28		(4)
M82	29 ± 0.2	130	IRAM 30 m	0.82	29.5	$T_{\rm mb}$	(1)
Maffei 2	13.8 ± 0.9	...	NRO 45 m	0.54	19	$T_{\rm mb}$	(3)
NGC 34	1.6 ± 0.2	600-700	SEST 15 m	0.75	57	$T_{\rm mb}$	(6)
NGC 253	40.8	150	NRO 45 m	0.45	23		(7)
NGC 613	0.33 ± 0.2	130	SEST 15 m	0.75	57		(8)
NGC 1056	...	...		...	...		N/A[c]
NGC 1068	24.5 ± 0.9	220	IRAM 30 m	0.82	29.5	$T_{\rm mb}$	(1)
NGC 1365	6.0 ± 0.1	300-400	SEST 15 m	0.75	57	$T_{\rm mb}$	(6)
NGC 1377	0.47 ± 0.3	140	IRAM 30 m	0.80	28		(8)
NGC 1614	0.37	...	SEST 15 m	0.75	56		(9)
NGC 1614	1.5 ± 0.22	300	FCRAO 14 m	0.60	50		(5)
NGC 1808	2	...	SEST 15 m	0.75	56		(9)
NGC 2146	5 ± 0.1	290	IRAM 30 m	0.82	29.5	$T_{\rm mb}$	(1)
NGC 2623	1.1	300	OVRO array	...	...		(10), (11)
NGC 3079	4.2 ± 0.4	420	IRAM 30 m	0.80	28		(8)[d]
NGC 3079	2.6 ± 0.42	365	NRAO 12 m	0.89	72	$T_{\rm R}^*$	(5)
NGC 3256	2.3 ± 0.4	165	SEST 15 m	0.77	57	$T_{\rm mb}$	(12)
NGC 3690	2.04 ± 0.11	300	IRAM 30 m	0.82	28		(4)
NGC 4418	1.95 ± 0.12	170	IRAM 30 m	0.80	28		(8)
NGC 4945	22.4 ± 0.4	305	SEST 15 m	0.75	55	$T_{\rm mb}$	(13)
NGC 5135	0.65 ± 0.07	50-60	SEST 15 m	0.75	57	$T_{\rm mb}$	(6)
NGC 6946	8.7 ± 0.9	...	NRO 45 m	0.54	19	$T_{\rm mb}$	(3)
NGC 7130	0.7 ± 0.1	100	SEST 15 m	0.75	57	$T_{\rm mb}$	(6)
UGC 5101	1.40 ± 0.14	500	IRAM 30 m	0.82	28		(4)

[a] Integrated intensities are in $T_{\rm A}^*$ (if not stated differently) and in K km s^{-1}.

[b] (1) Krips et al. (2008), (2) Curran et al. (2001a), (3) Sorai et al. (2002), (4) Graciá-Carpio et al. (2008), (5) Gao & Solomon (2004), (6) Curran et al. (2000), (7) Nguyen-Q-Rieu et al. (1989), (8) This work, (9) Aalto et al. (1995), (10) Aalto et al. (2002), (11) Bryant (1996), (12) Casoli et al. (1992), (13) Wang et al. (2004).

[c] No HCN data were found in the literature for this object.

[d] These data were first published by Pérez-Beaupuits et al. (2007), but as the integrated intensities are not given, the data have been reduced again for this work.

Table 6.3. Data from HNC 1-0 measurements

Galaxy	I(HNC) 1-0[a] [K km s^{-1}]	Δv [km s^{-1}]	Telescope	$\eta_{\rm mb}$	$\theta_{\rm mb}$ [$''$]	T scale[a]	Reference[b]
Arp 220	0.95 ± 0.2	...	SEST 15 m	0.75	55		(1)
Circinus	1.87 ± 0.2	280	SEST 15 m	0.75	55		(2)
IC 342[c]	23 ± 3	40	OVRO array	...	5.9×5.1	$T_{\rm mb}$	(3)
IC 342	9.2 ± 0.7	47	IRAM 30 m	0.8	25	$T_{\rm R}^*$	(4)
IC 694	0.75 ± 0.2	300-400	OSO 20 m	0.59	42		(1)
IC 860	0.70 ± 0.09	230	IRAM 30 m	0.80	28		(2)
I17208	1.12 ± 0.1	350	IRAM 30 m	0.80	28		(2)
M82	7.3 ± 0.6	129	IRAM 30 m	0.64	25	$T_{\rm mb}$	(5)
Maffei 2	7.3 ± 0.8	91, 50	IRAM 30 m	0.64	25	$T_{\rm mb}$	(5)
NGC 34	< 0.44	...	SEST 15 m	0.75	55		(2)
NGC 253	50.0 ± 2.8	72, 136	IRAM 30 m	0.64	25	$T_{\rm mb}$	(5)
NGC 613	< 0.24	...	SEST 15 m	0.75	55		(2)
NGC 1056	< 0.17	...	IRAM 30 m	0.80	28		(2)
NGC 1068	1.57 ± 0.2	260	SEST 15 m	0.75	55		(2)[d]
NGC 1068	11.4 ± 0.7	232	IRAM 30 m	0.64	25	$T_{\rm mb}$	(5)
NGC 1365	3.2 ± 0.3	150	SEST 15 m	0.75	55		(2)[d]
NGC 1377	< 0.15	...	IRAM 30 m	0.80	28		(2)
NGC 1614	< 0.38	...	SEST 15 m	0.75	55		(2)
NGC 1808	1.2 ± 0.1	300	SEST 15 m	0.75	55		(1)
NGC 2146	1.6 ± 0.3	237	IRAM 30 m	0.64	25	$T_{\rm mb}$	(5)
NGC 2623	0.6 ± 0.15	500-600	OSO 20 m	0.59	42		(1)
NGC 3079	1.83 ± 0.33	380	IRAM 30 m	0.80	28		(2)[d]
NGC 3079	6.9 ± 1.0	545	IRAM 30 m	0.64	25	$T_{\rm mb}$	(5)
NGC 3256	0.6 ± 0.05	250	SEST 15 m	0.75	55		(1)
NGC 3690	...	...		...	...		N/A[e]
NGC 4418	1.24 ± 0.12	156	IRAM 30 m	0.77	27		(6)
NGC 4945	8.6 ± 0.5	290	SEST 15 m	0.75	55		(2)
NGC 5135	< 0.13	...	SEST 15 m	0.75	55		(2)
NGC 6946	4.0 ± 0.3	138	IRAM 30 m	0.64	25	$T_{\rm mb}$	(5)
NGC 7130	0.4 ± 0.05	...	SEST 15 m	0.75	55		(1)
UGC 5101	1.24 ± 0.20	...	IRAM 30 m	0.80	28		(2)

[a] Integrated intensities are in $T_{\rm A}^*$ (if not stated differently) and in K km s^{-1}. Upper limits are all 2σ.

[b] (1) Aalto et al. (2002), (2) This work, (3) Meier & Turner (2005), (4) Henkel et al. (1988), (5) Hüttemeister et al. (1995), (6) Aalto et al. (2007a).

[c] In the region with highest HC_3N value.

[d] These data were first published by Pérez-Beaupuits et al. (2007), but as the integrated intensities are not given, the data have been reduced again for this work.

[e] No HNC data were found in the literature for this object.

When calculating the brightness temperature of the source, the size of the source as well as the beam must be accounted for (see Equations 5.1 and 5.3):

$$T_{\rm B} = \frac{T_{\rm A}^*}{\eta_{\rm mb}} \cdot \frac{\theta_{\rm s}^2 + \theta_{\rm mb}^2}{\theta_{\rm s}^2}. \tag{6.1}$$

This is valid only if the source and beam are Gaussian shaped. $\theta_{\rm mb}$ is the main beam size of the telescope, $\eta_{\rm mb}$ is the main beam efficiency of the telescope and $\theta_{\rm s}$ is the source size. We assume that the source sizes are equal for the two transitions, as the transitions compared in this report probably come from the same regions, or at least regions with similar sizes.

Below, the ratio of transition A and transition B given the telescope parameters $\theta_{\rm mb}$ and $\eta_{\rm mb}$ is produced.

$$\frac{I({\rm A})}{I({\rm B})} = \frac{\theta_{\rm mbA}^2 + \theta_s^2}{\theta_{\rm mbB}^2 + \theta_{\rm s}^2} \frac{\eta_{\rm mbB}}{\eta_{\rm mbA}} \frac{\int T_{\rm AA}^* dv}{\int T_{\rm AB}^* dv}, \tag{6.2}$$

where $\int T_{\rm A}^* dv$ is the integrated intensity of the signal. Note that the temperature can also be given in $T_{\rm mb}$ scale – in this case, the main beam efficiency corresponding to that measurement should be omitted, since $T_{\rm mb} = \frac{T_{\rm A}^*}{\eta_{\rm mb}}$ (Equation 5.3).

6.2.1 When the source size is unknown

The source sizes used in this study are found in Table 5.1. However, for some sources no reliable value for the source size has been found. I will here discuss why this is not always a problem, and estimate sizes of the errors inflicted from not knowing the source size.

As can be seen above, the line ratios depend on the source and beam sizes with the factor $\frac{\theta_{\rm mbA}^2+\theta_{\rm s}^2}{\theta_{\rm mbA}^2+\theta_{\rm s}^2}$. The source size $\theta_{\rm s}$ can of course be ignored if both beam sizes $\theta_{\rm mbA}, \theta_{\rm mbB} \gg \theta_{\rm s}$. If the beam sizes $\theta_{\rm mbA} \approx \theta_{\rm mbB}$, the source size will also cancel. However, if $\theta_{\rm s}$ is considerably large, and $\theta_{\rm mbA}$ and $\theta_{\rm mbB}$ are non-similar, the source size becomes an important factor.

The error when assuming the source to be point-like, e.g. setting $\theta_{\rm s} = 0$, will be

$$\frac{\theta_{\rm mbA}^2/\theta_{\rm mbB}^2}{\frac{\theta_{\rm mbA}^2+\theta_{\rm s}^2}{\theta_{\rm mbB}^2+\theta_{\rm s}^2}}. \tag{6.3}$$

For the sources where an HCN source size has been used, the corresponding source diameter has never exceeded 1.6 kpc (NGC 2146). For the CO source sizes, the largest is found in NGC 5135, with a source diameter of 4.1 kpc in CO 1-0, but the HCN source sizes should be smaller than this.

Assuming no larger HCN source diameter than 1.6 kpc, and the largest and smallest beam sizes at 90 GHz (SEST with 57″ and IRAM with 28″), the error will be less than 5 % for distances larger than 45 Mpc, and less than 10 % for distances larger than 30 Mpc. For objects closer than 30 Mpc, the error thus is noticeable if the point-like approximation ($\theta_{\rm s} = 0$) is used, as long as the $\theta_{\rm mb}$ of the two measurements used to calculate the ratio are of notably different sizes.

6.2.2 Ratios between HCN, HNC and HC_3N lines

The calculated line ratios are shown in Table 6.4. Note that preference has been given to HC_3N 10-9 lines before other HC_3N lines. Only if no 10-9 line is available, another HC_3N line has been used for the ratios, specified in the footnotes.

Also note that a few of the galaxies appear twice in Table 6.4. This is where several values have been found for the same transition. As can be seen, the values on these measurements do not always agree, and the priority has to be given to some measurements before other. If the HC_3N and HNC data are found in the same spectrum in one of the measurements, preference has been given to this measurement, as it will increase the accuracy on the HC_3N/HNC ratio. In all other cases, the spectrum of each measurement has been investigated (when available), and the values from the spectrum with the lowest noise level has been put first in Table 6.4.

The fact that the intensities of two measurements on the same spectral line in the same source can be so different is further discussed in Appendix A.

6.2.3 HC_3N-luminous galaxies

I now try to establish a definition of an HC_3N-luminous galaxy. As HCN is the most common dense gas tracer, and also should be a more stable component of the dense gas than HNC, I decide to use the HC_3N/HCN ratios for this definition. It seems like most galaxies have an HC_3N/HCN ratio below 0.15, with the exception for a few interesting galaxies. Thus, $\frac{I(HC_3N)}{I(HCN)} < 0.15$ is set to be the limit for HC_3N-luminous galaxies. If a corresponding limit should be set on the HC_3N/HNC ratio, it would be around 0.25 to include the same galaxies.

The galaxies thus seen as HC_3N-luminous or HC_3N-rich are NGC 4418, IC 342, Maffei 2, Circinus, M82, Arp 220, I17208 and possibly NGC 3079. I also choose to include IC 860, considering that its moderate HC_3N value ($\frac{I(HC_3N)}{I(HNC)} = 0.11$) is in the 28-27 transition, as the higher transition lines seem to be weaker than the 10-9 line in most galaxies where more than one line has been measured (when beam effects are compensated for). A few of these galaxies are quite nearby, and as will be discussed in the next chapter, the HC_3N/HCN ratio of galaxies with source sizes larger than the telescope beam size will probably be overestimated. This is particularly the case for M82, IC 342 and Maffei 2.

Some galaxies can definitely be seen as HC_3N-poor, since their HC_3N/HCN ratio is less than or equal to 0.10: NGC 253, NGC 1068, NGC 1808, NGC 3256, NGC 4945, NGC 6946 and UGC 5101. Since NGC 253 also belongs to the nearby galaxies, this value should probably be even lower.

6.3 Rotation diagrams

The temperature in a gas cloud can be estimated in a rotation diagram if the intensities of several rotational transitions of the same molecule are known. A short presentation of rotation diagrams can be found in Nummelin (1998).

A rotation diagram for temperature estimation of HC_3N in NGC 253 is found in Martín et al. (2006). The rotational temperature is estimated to 24-33 K. By using

Table 6.4. Line ratios

Galaxy	$\frac{I(HC_3N\ 10-9)}{I(HCN\ 1-0)}$	$\frac{I(HC_3N\ 10-9)}{I(HNC\ 1-0)}$	$\frac{I(HNC\ 1-0)}{I(HCN\ 1-0)}$
Arp 220	0.19 ± 0.08[a]	0.42 ± 0.3[a]	0.45 ± 0.1
Arp 220	0.78 ± 0.15[b]	1.73 ± 0.7[b]	0.45 ± 0.1
Circinus	0.24 ± 0.1	0.54 ± 0.2	0.45 ± 0.1
IC 342	0.28 ± 0.1[c]	0.27 ± 0.1[c]	1.00 ± 0.15[c]
IC 694	< 0.60[d]	< 0.34[d]	1.79 ± 0.6
IC 860	...	0.11 ± 0.05[e]	...
I17208	0.15 ± 0.04[f]	0.29 ± 0.08	0.52 ± 0.09[f]
I17208	0.06 ± 0.03[g]	0.29 ± 0.08	0.21 ± 0.08[g]
Maffei 2	0.26[d]	0.32[d]	0.81 ± 0.15
M82	0.21 ± 0.02	0.96 ± 0.2	0.22 ± 0.02
NGC 34	< 0.35	...	< 0.34
NGC 253	0.08 ± 0.008	0.12 ± 0.02	0.63 ± 0.04
NGC 613	< 0.75	...	< 0.69
NGC 1056	...	...	...
NGC 1068	0.053 ± 0.05	0.22 ± 0.2	0.24 ± 0.04
NGC 1365	< 0.13	< 0.19	0.67 ± 0.06
NGC 1377	< 0.26[h]	...	< 0.32
NGC 1614	< 0.25[g]	...	< 0.24[g]
NGC 1614	< 1.02[i]	...	< 0.99[i]
NGC 1808	0.10 ± 0.05	0.18 ± 0.1	0.58 ± 0.05
NGC 2146	< 0.22	< 0.85	0.26 ± 0.06
NGC 2623	< 0.50[d]	< 0.70[d]	0.71
NGC 3079	0.14 ± 0.04	0.33 ± 0.015	0.44 ± 0.13
NGC 3256	< 0.065	< 0.20	0.32 ± 0.1
NGC 3690	< 0.40[d]	...	...
NGC 4418	0.40 ± 0.07	0.65 ± 0.15	0.62 ± 0.1
NGC 4945	0.09 ± 0.01	0.17 ± 0.03	0.51 ± 0.04
NGC 5135	< 0.25	...	< 0.25
NGC 6946	< 0.065[d]	< 0.089[d]	0.72 ± 0.15
NGC 7130	< 0.18	< 0.25	0.71 ± 0.2
UGC 5101	< 0.09	< 0.1	0.91 ± 0.25

[a] HC_3N value from Aalto et al. (2002) used.
[b] HC_3N value from this work used.
[c] HC_3N and HNC values from Henkel et al. (1988) used.
[d] HC_3N 12-11 line.
[e] HC_3N 28-27 line.
[f] HCN value from Graciá-Carpio et al. (2008) used.
[g] HCN value from Gao & Solomon (2004) used.
[h] HC_3N 16-15 line.
[i] HCN value from Aalto et al. (1995) used.

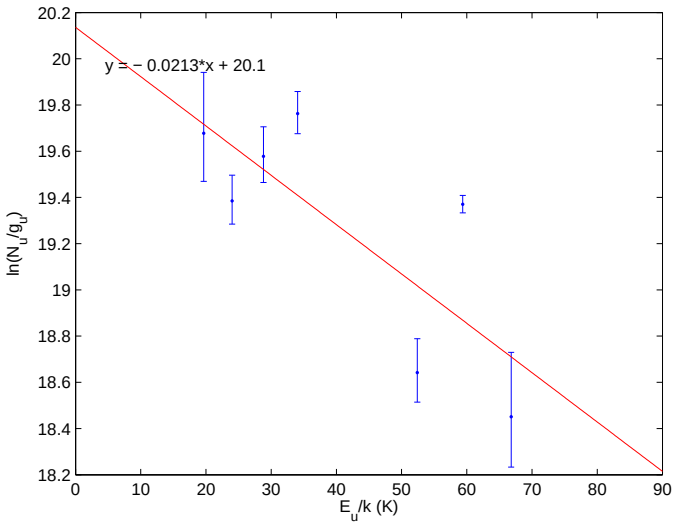

Figure 6.1. The rotation diagram for NGC 4945.

HC_3N values on NGC 4945 from Wang et al. (2004), and data for HC_3N emission line properties found in the Leiden Atomic and Molecular Database (LAMDA – Schöier et al. 2005), we can put together a rotation diagram also for this galaxy. The result is shown in Figure 6.1. As can be seen, the interpolated inclination is -0.0213. In Nummelin (1998), we find that the rotational temperature of the molecules is the negative inverse to this inclination, or 47 K, thus somewhat hotter than in NGC 253.

Too few HC_3N lines are available to establish such a plot for any other galaxy in the sample (apart from NGC 4418 – but the LAMDA data only covers transitions up to $J = 21$, and only two measurements on such low transitions are available for this galaxy).

7 HIGH HC_3N/HCN RATIOS IN SOME NEARBY GALAXIES

For the most nearby galaxies in the study, the dense molecular gas regions subtends an angle on the sky of the same order as or larger than the telescope beam size. If the region with the measured gas actually extends wider than the beam size, a global value of the galaxy's intensity for that molecule will no longer be measured, but rather the intensity for a central region.

When calculating molecular ratios, this might pose a problem. Only if we expect the distributions of the two molecules to be of the same shape and size, we will achieve the same ratio as for a global measurement on the galaxy. In particular, we expect the HC_3N to be concentrated in a smaller region of the galaxy than HCN and HNC (see e.g. Meier & Turner (2005)), why the calculations of these ratios depend on the beam size to be large enough to cover the whole dense region of the galaxy (e.g. the whole HCN region).

If the beam size is smaller than the HCN (or HNC) region, but larger than the HC_3N region, the HC_3N/HCN (or HC_3N/HNC) ratio will be overestimated, as all HC_3N will be seen, but not all HCN (or HNC).

The galaxies in our survey that do not fulfil the criterion $\theta_s \lesssim \theta_{mb}$ are IC 342, M82, Maffei 2 and NGC 253, and we therefore expect the real HC_3N/HCN ratios to be somewhat lower for these galaxies. Thus, IC 342, M82 and Maffei 2 maybe should not be considered being globally HC_3N-luminous, even though they fulfil the HC_3N/HCN ratio criterion in a small beam covering the central region.

Note that not knowing the HC_3N source size will also affect the line ratios from the more distant galaxies to some extent, since the source size used for the line ratio calculations is an HCN source size (in a few cases even a CO source size) also for the HC_3N intensities. However, assuming the proportion between the HCN and HC_3N source sizes to be similar for all galaxies, this will affect all line ratios in the same way, thus making all line ratios a little bit too high.

Another problem for the line ratios of the nearby galaxies is that the two different measurements used to calculate a line ratio sometimes are taken with different beam sizes. When comparing HCN 1-0, HNC 1-0 and HC_3N 10-9 measurements taken with the same telescopes, the difference in source size is negligible, but if a line ratio is calculated from measurements from two different telescopes, the two molecular intensities are measured in regions with different sizes. For distant galaxies this is not a problem, since the whole molecular region of the galaxy is unresolved in any beam. For the more nearby galaxies, one of the molecules might be measured more or less globally in the galaxy, while the other is measured very locally in the galactic centre, giving an erroneous line ratio.

8 POSSIBLE CORRELATIONS

Initially, is was surprising to find substantial emission from a molecule as "fragile" as HC_3N in galaxies with extremely strong radiation, probably either being starbursts with strong UV emission or AGN galaxies with strong UV and X-ray emission. However, very recent preliminary models of the chemistry in such objects (e.g. NGC 4418) have shown that HC_3N actually may survive to a detectable level in both XDRs and PDRs, and actually somewhat better in XDRs than in PDRs (Costagliola & Aalto in prep.).

The sample was made to find many HC_3N-luminous galaxies, but many of these were found to be HC_3N-poor. This could mean one of three things:

- Our search-criteria for HC_3N-rich galaxies are bad.
- HC_3N-luminous galaxies are very rare, even among active galaxies.
- The limit for HC_3N-luminous galaxies is set too high to include all interesting objects.

Several possible correlations between a high HC_3N intensity and other properties of the galaxies have been examined. This will be discussed below.

8.1 Starbursts or AGNs?

If the HC_3N-rich and -poor galaxies from Section 6.2.3 are compared with the galaxy classifications of Table 5.2, the most obvious trend is that most of the HC_3N-poor galaxies are starbursts, with the exception for the LIRG UGC 5101.

If the nearby galaxies are removed from the HC_3N-rich category (see Chapter 7), the remaining galaxies' common denominator seems to be that their source of activity is unknown or disputed – they are labelled as "obscured" or ULIRGs. Thus, HC_3N might thrive in deeply obscured, shielded regions, where it cannot be destroyed by radiation. In starbursts, it is destroyed by the strong UV field – or not even created, as C_2H_2 on the grains will photo-dissociate into C_2H (see Section 3.4).

8.2 PAHs and silicates

In Spoon et al. (2002), several absorption features from ice and silicates as well as emission from PAHs in active galaxies are discussed. In Spoon et al. (2007), an evolutionary plot for active galaxies is produced, showing two distinct regions in a plot over the equivalent width of the PAH 6.2 µm emission line versus the strength of the silicate 9.7 µm absorption line. Starburst galaxies tend to have a high PAH width, Seyfert galaxies have low PAH width and low silicate strength, while ULIRGs have high silicate strength and often also low PAH width.

This is partly explained by PAHs thriving in PDRs, but being destroyed by the strong radiation from AGNs. However, sometimes starbursts are so heavily obscured

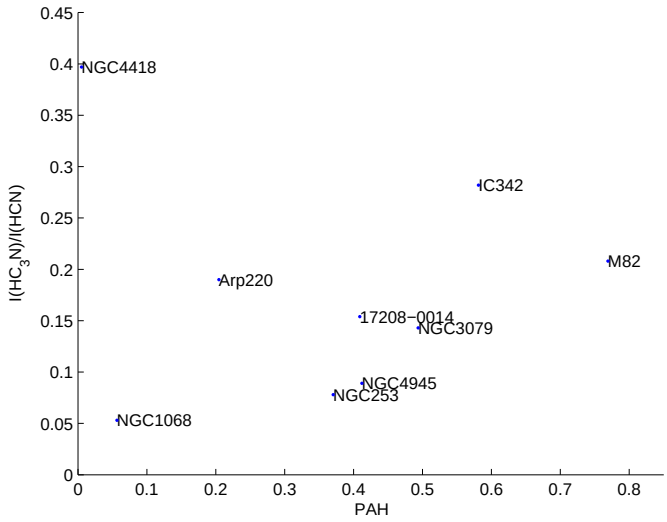

Figure 8.1. Tentative correlation between HC_3N/HCN ratio and PAH width. HC_3N/HCN values for IC 342 and Maffei 2 are probably overestimated (see Chapter 7).

by dust that the PAH emission will be absorbed, and thus a low PAH level should not always indicate AGN presence.

By private communication with H. W. W. Spoon, the numerical values for all the galaxies in his sample were obtained. Most galaxies in our sample is also included in his sample. When comparing these values to our HC_3N/HCN ratios, a tentative pattern could be detected.

In Figures 8.1 and 8.2 the plots with the relations between the HC_3N/HCN ratio, the PAH width, and the silicate strength are shown. Note that two of the three nearby galaxies in the sample, M82 and IC 342, are showing too high HC_3N/HCN ratios to fit into the pattern of both figures, which was expected (see Chapter 7).

In Figure 8.1, Arp 220 and NGC 4418 also break the pattern. These two objects could be part of another population than the other objects in the sample – the HC_3N in these galaxies with deeply obscured cores might come from regions shielded from the central power source, while the HC_3N in the other objects come from PDRs also containing PAHs from star formation, as most of them are starburst galaxies.

In Figure 8.2, a correlation between HC_3N luminosity and the silicate strength seems possible. Note that the silicate strength is in a magnitude scale, higher numbers thus meaning weaker silicate absorption. One explanation to the correlation might be that HC_3N is formed in regions with silicates, where the silicates protect the HC_3N from radiation. Thus, HC_3N survives better in regions with high silicate abundance.

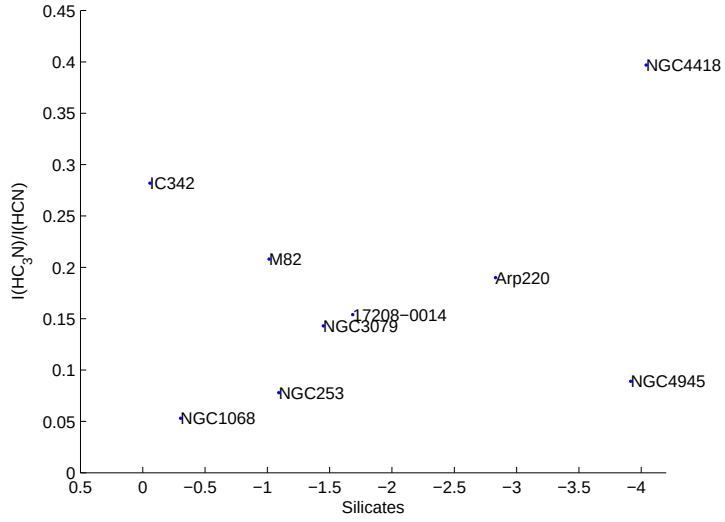

Figure 8.2. Tentative correlation between HC_3N/HCN ratio and silicate strength. HC_3N/HCN values for IC 342 and Maffei 2 are probably overestimated (see Chapter 7). Note that a high value on the silicate strength means low silicate abundance.

8.3 Megamasers

Neglecting the most nearby galaxies, where the HC_3N/HCN ratios probably are somewhat exaggerated (see Chapter 7), all HC_3N-luminous galaxies have OH mega- or kilomasers (Darling & Giovanelli 2006), except for NGC 3079, which has an H_2O megamaser (Satoh et al. 1997). A few of the HC_3N-poor galaxies also have OH mega- or kilomaser activity (NGC 253, NGC 1068 and UGC 5101). The concept of defining megamaser strength only from its luminosity may however be somewhat misleading. Firstly, a galaxy with much molecular gas is more likely to harbour a strong megamaser than one with little molecular gas (Darling 2007). Secondly, since we want to compare the OH megamaser luminosities with a ratio between two line intensities, it is more reasonable to normalise the OH megamaser luminosity with some kind of luminosity for the molecular gas in the galaxy. I have chosen to use the CO 1-0 luminosity for this, since CO traces molecular gas (see Section 3.1).

For IC 860, no CO 1-0 luminosity value has been found in the literature, but from a measurement performed with the IRAM 30 m telescope by F. Costagliola the luminosity could be calculated from the intensity with the method described in Solomon et al. (1997). The intensity 9.83 K km/s, the beam width 22″ and the distance 59.1 Mpc gives a luminosity of $3.07 \cdot 10^8$ K km s^{-1} pc^2, assuming that the source size is much smaller than the beam size, which is valid for IC 860.

A lin-log-plot of the ratios is shown in Figure 8.3. The correlation is just tentative, but maybe the most important correlation is that between strong HC_3N luminosity and the existence of a strong OH (mega)maser.

We can see that UGC 5101 is the only HC_3N-poor galaxy with an OH megamaser that is strong as compared to the amount of molecular gas in the galaxy. It might

Table 8.1. OH maser luminosities and CO luminosities for some of the sources in the sample. Data from Darling (2007) unless stated otherwise in the footnotes.

Galaxy	$\log L_{\rm OH}$ $[L_\odot]$	$L_{\rm CO1-0}$ $[10^8$ K km s^{-1} pc$^2]$
Arp 220	2.58	78.5
IC 694/NGC 3690	1.38	29
IC 860	0.27[a]	3.07[b]
I17208	3.04	146.9
M82	-1.7	5.7
NGC 253	-1.3	4.6
NGC 1068	-0.3	20.7
NGC 4418	0.04[a]	1.03[c]
UGC 5101	1.61	50.8

[a] From Darling & Giovanelli (2002).
[b] From measurements by F. Costagliola.
[c] From Albrecht et al. (2007).

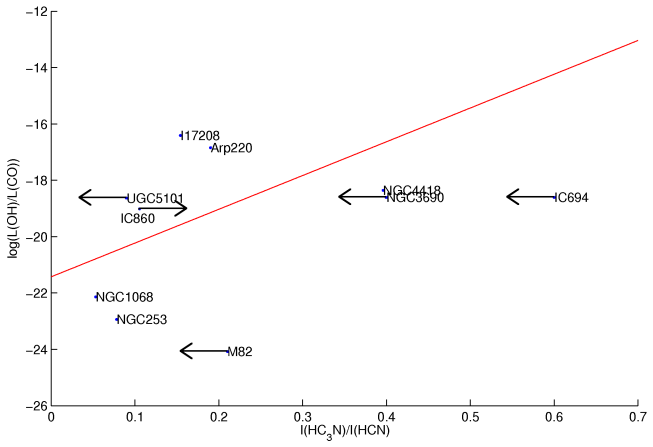

Figure 8.3. $\log \frac{L_{\rm OH}}{L_{\rm CO}}$ as a function of HC_3N/HCN. The HC_3N values for IC 694, NGC 3690 and UGC 5101 are upper limits, and the HC_3N/HCN value for M82 should also be seen as an upper limit, since it is nearby. The HC_3N/HCN value for IC 860 should be seen as a lower limit, since it is taken for the 28-27 line, and not the 10-9 line. The data points with upper or lower limits have not been included in the line interpolation.

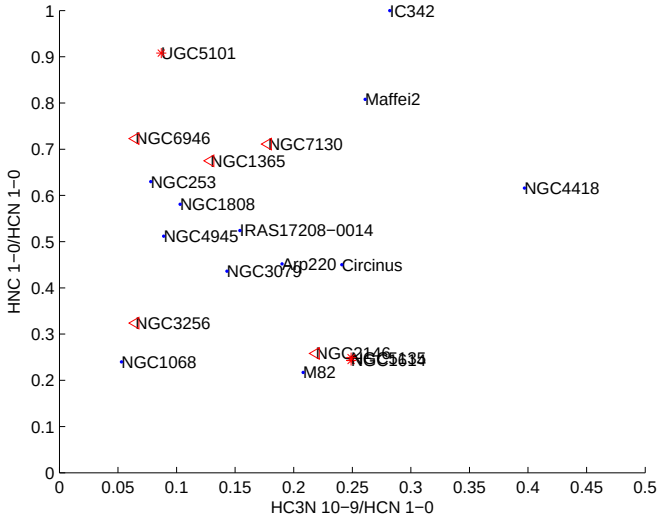

Figure 8.4. HC_3N/HCN ratio versus HNC/HCN 1-0 ratio. Red arrow-shaped data points are upper limits on HC_3N/HCN ratio. Red star-shaped data points are upper limits on both the HC_3N/HCN and the HNC/HCN ratios.

be interesting to note that when performing HC_3N measurements on UGC 5101, a signal was first detected, but this detection was not reproduced the following days of observation. Neither did recent measurements (June 2009) performed at the IRAM 30 m telescope show any HC_3N signal from UGC 5101. These data are still to be published.

The OH/CO ratio could be an exponential function of the HC_3N/HCN ratio, higher HC_3N levels giving stronger OH masers as compared to the amount of molecular gas.

A possible explanation is that warm dust may help protect HC_3N from destructive UV radiation, and also create an IR field which will both excite the HC_3N and power the OH megamaser. According to Darling & Giovanelli (2006), warm dust is needed for formation of OH megamasers .

8.4 HNC/HCN

As can be seen in Figures 8.4-8.5, both the HC_3N/HCN and HC_3N/HNC ratios seem to be unrelated to the HNC/HCN 1-0 ratio.

Attempts were also made trying to find a correlation between the HC_3N ratios and ratios of higher HNC and HCN transitions, e.g. the HNC/HCN 3-2 ratio. However, too few HNC 3-2 and HCN 3-2 spectra for the galaxies in the sample are available in the literature – with only five data points no conclusions can be drawn, especially considering that the HCN 3-2 and HNC 3-2 seem to be very uncertain, at least for Arp 220 and NGC 4418. This is further discussed in Appendix A.

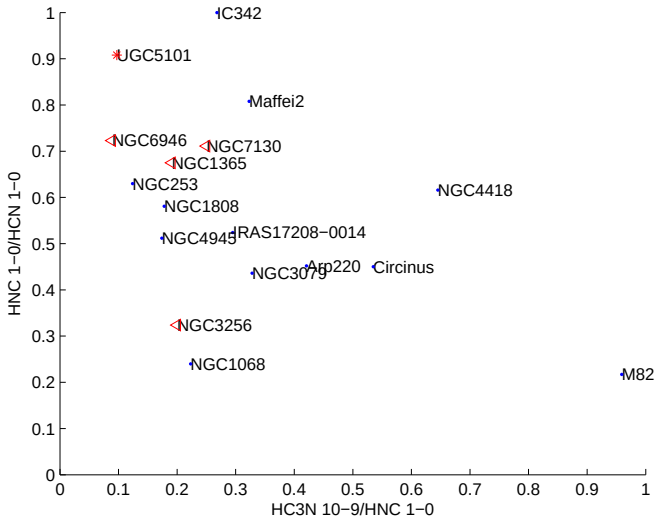

Figure 8.5. HC_3N/HNC ratio versus HNC/HCN 1-0 ratio. Red arrow-shaped data points are upper limits on HC_3N/HNC ratio. Red star-shaped data points are upper limits on both the HC_3N/HNC ratio and the HNC/HCN ratio.

8.5 HC_3N and C_2H – some recent updates

As discussed in Section 3.4, C_2H_2 present in grains in the interstellar medium might either photo-dissociate to form C_2H or react with CN to form HC_3N. If this is the mechanism that forms HC_3N in the HC_3N-luminous galaxies, and C_2H_2 can be assumed to be present in most grain-chemistries, this would suggest that a strong C_2H line should be found in galaxies without strong HC_3N lines.

Also, in Meier & Turner (2005), where IC 342 is mapped in several different molecules, it is clearly visible that HC_3N and C_2H exist in different parts of the galaxy – they seem to exclude each other in a way no other molecules in the mappings do.

Further on, HC_3N seems to be either a quite uncommon molecule, or normally too weak to be detected, since it was not detected in most of the studied objects (which is strengthened by the recent measurements mentioned above). In the future we will calculate the expected HC_3N luminosity assuming a normal "Orion-like" abundance and cloud conditions derived from other high density tracers.

If HC_3N really is uncommon, it can be explained in several different ways: The galaxies without HC_3N might have a lack of C_2H_2 or CN, or they have a strong UV field that dissociates C_2H_2 too quick for it to react with CN; or perhaps a strong source of radiation that dissociates the HC_3N. As C_2H_2 is hard to study since it has no rotational transitions, it would be interesting to investigate the C_2H abundance in galaxies where the HC_3N abundance has been studied – this was started in the IRAM measurements of June 2009.

8.6 Future observational tests

It would be interesting to run further tests investigating the possible correlations outlined in this chapter. Further analysis of the recent IRAM measurements could possibly confirm the connection between HC_3N and C_2H abundances.

HC_3N data on more sources in Spoon's sample are needed to confirm any correlations between the HC_3N/HCN ratio and PAH and/or silicate abundances.

It would also be interesting to do mapping of HC_3N, C_2H, HCN and HNC in more galaxies, to compare the results with the maps of IC 342 in Meier & Turner (2005).

9 HIGH HC_3N ABUNDANCE OR PUMPING?

The high HC_3N luminosity measured in some galaxies of course indicates that HC_3N should be rather abundant in these galaxies. This is, however, a too quick conclusion. It is possible that the spectral lines are pumped by infrared radiation, thus producing more emission than would be expected from a given molecular abundance (see Section 2.3).

9.1 Calculating the critical density

To investigate whether the HC_3N emission from the sources is dominated by transmission created by collisional excitation or by radiated pumping, a critical density below which the excitations of the molecules are dominated by radiation must be determined. The calculations below will follow directions and use formulae given in Rohlfs & Wilson (2004).

Assuming local thermal equilibrium (LTE), the Boltzmann equation can be used:

$$\frac{n_u}{n_l} = \frac{g_u}{g_l} e^{-\frac{h\nu}{kT_{\rm ex}}}, \tag{9.1}$$

where n_u and n_l are the densities of the states u and l, g_u and g_l are their statistical weights, and $T_{\rm ex}$ is the excitation temperature, which equals the kinetic temperature $T_{\rm kin}$ and the radiation temperature $T_{\rm R}$ under the LTE approximation.

For a system in stationary state,

$$\frac{n_u}{n_l} = \frac{B_{lu} I}{B_{ul} I + A_{ul}}, \tag{9.2}$$

where A_{ul}, B_{lu} and B_{ul} are the Einstein coefficients of the transition. Note that $B_{ul} = B_{lu}\frac{g_l}{g_u}$. Using this, and Equations 9.1 and 9.2, we get

$$e^{-\frac{h\nu}{kT_{\rm ex}}} = \frac{B_{lu} I}{B_{ul} I + A_{ul}}, \tag{9.3}$$

which can be rewritten into

$$B_{ul} I = \frac{A_{ul}}{e^{\frac{h\nu}{kT_{\rm ex}}} - 1}, \tag{9.4}$$

which is the pumping rate.

The collisional rate is simply

$$C_{lu} = n(H_2) \cdot q_{lu}. \tag{9.5}$$

The critical density is the density for which the collision rate C_{lu} equals the pumping rate $B_{ul} I$. Combining Equations 9.4 and 9.5, the critical density is given as

$$n(\mathrm{H_2})^* = \frac{A_{ul}}{e^{\frac{h\nu}{kT_{\mathrm{ex}}}} - 1} \cdot \frac{1}{q_{ul}}. \tag{9.6}$$

Using data from the Leiden Atomic and Molecular Database (LAMDA – Schöier et al. 2005) and Wyrowski et al. (1999), the critical densities were calculated for the three lowest vibrational states of HC_3N (v_7, v_6 and v_5) with the four temperatures available in LAMDA (10 K, 20 K, 40 K and 80 K). The dust temperature of NGC 4418 is estimated to 85 K in Evans et al. (2003), why these temperatures seem to be realistic. For all the vibrational (pumping) transitions, and for all these temperatures, the critical densities lie around 10^5 cm^{-3}.

Calculations to determine abundances of several dense gas tracers (HCN, HNC, CS and HCO^+) in NGC 4418 performed by F. Costagliola (private communication) using RADEX, a statistical equilibrium radiative transfer code (van der Tak et al. 2007), show that the H_2 abundance is of the order 10^5-10^6 cm^{-3}. As the H_2 abundances agree for all the dense gas tracers, it is reasonable to believe that it is correct also for HC_3N, if the HC_3N emission comes from the same dense gas areas. If so, the collisional excitations are of at least the same order as the pumping, and the HC_3N emission does not need to be dominated by pumping. There are, however, signs of pumping in NGC 4418, Arp 220 and IC 860, as vibrational HC_3N transitions recently have been discovered in these galaxies (Costagliola & Aalto in prep.).

The critical densities are only calculated for HC_3N transitions up to $J = 21$ (as LAMDA has no data for higher HC_3N transitions), but the critical density is inversely related to J, and thus the emission from the higher transitions will also be dominated by collisions and not infrared pumping.

This does not tell anything about the HC_3N levels in the other galaxies in the sample – their properties could be (and are probably) somewhat or completely different from the properties of NGC 4418 – which always seems to be the odd one out regarding HC_3N. However, it can be concluded that the HC_3N emission in the most HC_3N-luminous galaxy is not dominated by pumping.

To perform the same calculations on other galaxies, more HC_3N spectral lines need to be measured, since the excitation temperature is derived from the relation between several spectral lines. Sufficient data are only available for NGC 253 and NGC 4945, neither being HC_3N-luminous galaxies.

10 CONCLUSIONS

Measurements of cyanoacetylene, HC_3N, in AGN galaxies and starburst galaxies indicate that high abundances of this molecule is relatively uncommon, but in a few galaxies can be comparable with HCN and HNC in intensity. It is possible that the HC_3N forms from acetylene, C_2H_2, boiling off from the grains in the interstellar medium and reacting with CN radicals. Where a strong UV field is present, the C_2H_2 will instead photo-dissociate into C_2H (ethynyl radicals), a theory supported by recent measurements.

A tentative connection between the HC_3N/HCN ratio and the level of PAHs in the galaxy has been found, indicating that both might be tracers of early star formation. However, the correlation does not apply to the most HC_3N-luminous galaxies (NGC 4418 and Arp 220), which both have low PAH levels. In these cases, the HC_3N might survive as the high obscuration in the galaxy shields it from the central power source.

A tentative connection between the HC_3N/HCN and silicate absorption has also been discovered. A possible explanation is that the silicates shield the HC_3N from radiation that would otherwise destroy it.

It also seems like galaxies with strong OH megamaser activity are more likely to be HC_3N-luminous. This could be explained by OH megamasers needing warm dust to shape, and HC_3N being protected and excited by warm dust.

Finally, no connection between the HC_3N/HCN and HNC/HCN ratios has been found.

10.1 Future work

More measurements of the HC_3N rate in active galaxies are needed to develop the possibility of using this molecule as an indicator of the source of activity. Such measurements were made with the IRAM telescope in June 2009 (principal investigator F. Costagliola). These data are yet to be analysed, but as the measurements were made with the new EMIR receiver, we hope that the quality of the data will be better. Also, as the EMIR receiver has a very high bandwidth, several spectral lines can be fit into the same spectrum, giving even better accuracies when calculation line ratios.

It would also be interesting to further investigate the abundance of HC_3N and other molecules in star forming regions in the Galaxy. This could give us knowledge about the chemistry of star formation, which could be important for the understanding of starburst galaxies.

Bibliography

Aalto, S. 2008, Ap&SS, 313, 273

Aalto, S., Booth, R. S., Black, J. H., & Johansson, L. E. B. 1995, A&A, 300, 369

Aalto, S., Monje, R., & Martín, S. 2007a, A&A, 475, 479

Aalto, S., Polatidis, A. G., Hüttemeister, S., & Curran, S. J. 2002, A&A, 381, 783

Aalto, S., Radford, S. J. E., Scoville, N. Z., & Sargent, A. I. 1997, ApJL, 475, L107

Aalto, S., Spaans, M., Wiedner, M. C., & Hüttemeister, S. 2007b, A&A, 464, 193

Aalto, S., Wilner, D., Spaans, M., et al. 2009, A&A, 493, 481

Adams, W. S. 1941, ApJ, 93, 11

Albrecht, M., Krügel, E., & Chini, R. 2007, A&A, 462, 575

Alton, P. B., Trewhella, M., Davies, J. I., et al. 1998, A&A, 335, 807

Baan, W. A. & Haschick, A. D. 1984, ApJ, 279, 541

Bajaja, E., Wielebinski, R., Reuter, H.-P., Harnett, J. I., & Hummel, E. 1995, A&AS, 114, 147

Barrett, A. H., Meeks, M. L., & Weinreb, S. 1964, AJ, 69, 134

Barrow, G. M. 1962, *Introduction to Molecular Spectroscopy*, McGraw-Hill, Tokyo. Fonds Lerch

Bergvall, N., Laurikainen, E., & Aalto, S. 2003, A&A, 405, 31

Bohme, D. K. & Raksit, A. B. 1985, MNRAS, 213, 717

Bryant, P. M. 1996, PhD thesis, Calif. Inst. Tech., Pasadena

Bryant, P. M. & Scoville, N. Z. 1999, AJ, 117, 2632

Carroll, B. W. & Ostlie, D. A. 2007, *An Introduction to Modern Astrophysics*, 2. edn, Pearson Addison-Wesley, San Francisco

Carroll, T. J. & Goldsmith, P. F. 1981, ApJ, 245, 891

Casoli, F., Dupraz, C., & Combes, F. 1992, A&A, 264, 49

Cernicharo, J., Pardo, J. R., & Weiss, A. 2006, ApJL, 646, L49

Chapman, J. F., Millar, T. J., Wardle, M., Burton, M. G., & Walsh, A. J. 2009, MNRAS, 394, 221

Cherchneff, I., Glassgold, A. E., & Mamon, G. A. 1993, ApJ, 410, 188

Cid Fernandes, R., Heckman, T., Schmitt, H., González Delgado, R. M., & Storchi-Bergmann, T. 2001, in *The Central Kiloparsec of Starbursts and AGN: The La Palma Connection*, J. H. Knapen, J. E. Beckman, I. Shlosman & T. J. Mahoney (Eds.), vol. 249 of *Astronomical Society of the Pacific Conference Series*, 536

Cid Fernandes, R. J., Storchi-Bergmann, T., & Schmitt, H. R. 1998, MNRAS, 297, 579

Conselice, C. J., Gallagher, J. S., Calzetti, D., Homeier, N., & Kinney, A. 2000, AJ, 119, 79

Costagliola, F. & Aalto, S. in prep.

Cox, C. V. 1995, PhD thesis, AA(THE UNIVERSITY OF MICHIGAN.)

Curran, S. J., Aalto, S., & Booth, R. S. 2000, A&AS, 141, 193

Curran, S. J., Johansson, L. E. B., Bergman, P., Heikkilä, A., & Aalto, S. 2001a, A&A, 367, 457

Curran, S. J., Polatidis, A. G., Aalto, S., & Booth, R. S. 2001b, A&A, 373, 459

Dale, D. A., Sheth, K., Helou, G., Regan, M. W., & Hüttemeister, S. 2005, AJ, 129, 2197

Darling, J. 2007, ApJL, 669, L9

Darling, J. & Giovanelli, R. 2002, AJ, 124, 100

Darling, J. & Giovanelli, R. 2006, AJ, 132, 2596

de Vicente, P., Martín-Pintado, J., Neri, R., & Colom, P. 2000, A&A, 361, 1058

Draine, B. T. 1985, in *NATO ASIC Proc. 157: Molecular Astrophysics: State of the Art and Future Directions*, G. H. F. Diercksen, W. F. Huebner, & P. W. Langhoff (Ed.), 295

Evans, A. S., Becklin, E. E., Scoville, N. Z., et al. 2003, AJ, 125, 2341

Farrah, D., Afonso, J., Efstathiou, A., et al. 2003, MNRAS, 343, 585

Förster Schreiber, N. M., Roussel, H., Sauvage, M., & Charmandaris, V. 2004, A&A, 419, 501

Fraunhofer, J. 1822, Astronomische Nachrichten, 1, 295

Fukuzawa, K. & Osamura, Y. 1997, ApJ, 489, 113

Gao, Y. & Solomon, P. M. 2004, ApJS, 152, 63

Genzel, R., Lutz, D., Moorwood, A. F. M., et al. 2000, in *ISO Survey of a Dusty Universe*, D. Lemke, M. Stickel & K. Wilke (Eds.), vol. 548 of *Lecture Notes in Physics, Berlin Springer Verlag*, 199

Graciá-Carpio, J., García-Burillo, S., Planesas, P., Fuente, A., & Usero, A. 2008, A&A, 479, 703

Greve, T. R., Papadopoulos, P. P., Gao, Y., & Radford, S. J. E. 2009, ApJ, 692, 1432

Hattori, T., Yoshida, M., Ohtani, H., et al. 2004, AJ, 127, 736

Heikkilä, A., Johansson, L. E. B., & Olofsson, H. 1999, A&A, 344, 817

Henkel, C., Matthews, H. E., Morris, M., Terebey, S., & Fich, M. 1985, A&A, 147, 143

Henkel, C., Schilke, P., & Mauersberger, R. 1988, A&A, 201, L23

Hüttemeister, S., Henkel, C., Mauersberger, R., et al. 1995, A&A, 295, 571

Imanishi, M. 2006b, AJ, 131, 2406

Imanishi, M., Nakanishi, K., & Kohno, K. 2006a, AJ, 131, 2888

Imanishi, M., Nakanishi, K., Tamura, Y., Oi, N., & Kohno, K. 2007, AJ, 134, 2366

Irvine, W. M., Goldsmith, P. F., & Hjalmarson, Å. 1987, in *Interstellar Processes*, D. J. Hollenbach & H. A. Thronson, Jr. (Eds.), vol. 134 of *Astrophysics and Space Science Library*, 561

Jansky, K. G. 1933, Nature, 132, 66

Jungwiert, B., Combes, F., & Axon, D. J. 1997, A&AS, 125, 479

Kartje, J. F., Königl, A., & Elitzur, M. 1999, ApJ, 513, 180

Kinney, A. L., Bohlin, R. C., Calzetti, D., Panagia, N., & Wyse, R. F. G. 1993, ApJS, 86, 5

Knudsen, K. K., Walter, F., Weiss, A., et al. 2007, ApJ, 666, 156

Koda, J., Sofue, Y., Kohno, K., et al. 2002, ApJ, 573, 105

Krips, M., Neri, R., García-Burillo, S., et al. 2008, ApJ, 677, 262

Lahuis, F., Spoon, H. W. W., Tielens, A. G. G. M., et al. 2007, ApJ, 659, 296

Lancon, A., Rocca-Volmerange, B., & Thuan, T. X. 1996, A&AS, 115, 253

Laor, A. 2004, in *AGN Physics with the Sloan Digital Sky Survey*, G. T. Richards & P. B. Hall (Eds.), vol. 311 of *Astronomical Society of the Pacific Conference Series*, 169

Lutz, D., Maiolino, R., Spoon, H. W. W., & Moorwood, A. F. M. 2004, A&A, 418, 465

Malhotra, S., Beichman, C. A., Helou, G., et al. 1996, in *Bulletin of the American Astronomical Society*, vol. 28 of *Bulletin of the American Astronomical Society*, 1356

Marcum, P. M., O'Connell, R. W., Fanelli, M. N., et al. 2001, ApJS, 132, 129

Martig, M. & Bournaud, F. 2008, MNRAS, 385, L38

Martín, S., Mauersberger, R., Martín-Pintado, J., Henkel, C., & García-Burillo, S. 2006, ApJS, 164, 450

Mason, A. M. & Wilson, C. D. 2004, ApJ, 612, 860

Mauersberger, R., Henkel, C., & Sage, L. J. 1990, A&A, 236, 63

Meier, D. S. & Turner, J. L. 2005, ApJ, 618, 259

Moorwood, A. F. M. & Glass, I. S. 1984, A&A, 135, 281

Morris, M., Snell, R. L., & vanden Bout, P. 1977, ApJ, 216, 738

NED 2009, NASA Extragalactic Database

Nguyen-Q-Rieu, Nakai, N., & Jackson, J. M. 1989, A&A, 220, 57

Nguyen-Rieu, Viallefond, F., Combes, F., et al. 1994, in *IAU Colloq. 140: Astronomy with Millimeter and Submillimeter Wave Interferometry*, M. Ishiguro & J. Welch (Eds.), vol. 59 of *Astronomical Society of the Pacific Conference Series*, 336

Norman, C. & Scoville, N. 1988, ApJ, 332, 124

Nummelin, A. 1998, PhD thesis, Chalmers Univ. Technol., Göteborg

Olsson, E. 2009, PhD thesis, Chalmers Univ. Technol., Göteborg

Orgel, L. E. 2002, Origins of Life and Evolution of Biospheres, 32, 279

Papadopoulos, P. P. 2007, ApJ, 656, 792

Papovich, C., Giavalisco, M., Dickinson, M., Conselice, C. J., & Ferguson, H. C. 2003, ApJ, 598, 827

Pérez-Beaupuits, J. P. 2006, HCN and HNC in Seyfert Galaxies, Master's thesis, Chalmers Univ. Technol., Göteborg

Pérez-Beaupuits, J. P., Aalto, S., & Gerebro, H. 2007, A&A, 476, 177

Radford, S. J. E., Delannoy, J., Downes, D., et al. 1991, in *Dynamics of Galaxies and Their Molecular Cloud Distributions*, F. Combes & F. Casoli (Eds.), vol. 146 of *IAU Symposium*, 303

Regan, M. W., Sheth, K., & Vogel, S. N. 1999, ApJ, 526, 97

Reunanen, J., Kotilainen, J. K., & Prieto, M. A. 2003, MNRAS, 343, 192

Rohlfs, K. & Wilson, T. L. 2004, *Tools of radio astronomy*, 4. rev. and enl. ed. edn, Springer, Berlin

Sagan, C., Khare, B. N., & Lewis, J. S. 1984, *Organic matter in the Saturn system*, 788–807. University of Arizona Press, Tucson

Sanders, D. & Ishida, C. 2004, in *The Neutral ISM in Starburst Galaxies*, S. Aalto, S. Huttemeister & A. Pedlar (Eds.), vol. 320 of *Astronomical Society of the Pacific Conference Series*, 230

Sanders, D. B., Mazzarella, J. M., Kim, D.-C., Surace, J. A., & Soifer, B. T. 2003, AJ, 126, 1607

Satoh, S., Inoue, M., Nakai, N., et al. 1997, The Megamaser-AGN Connection, 23rd meeting of the IAU, Joint Discussion 21, 26 August 1997, Kyoto, Japan, meeting abstract.

Schilke, P., Walmsley, C. M., Pineau Des Forets, G., et al. 1992, A&A, 256, 595

Schöier, F. L., van der Tak, F. F. S., van Dishoeck, E. F., & Black, J. H. 2005, A&A, 432, 369

Scoville, N. Z. & Sanders, D. B. 1987, in *Interstellar Processes*, D. J. Hollenbach & H. A. Thronson, Jr. (Eds.), vol. 134 of *Astrophysics and Space Science Library*, 21

Sheth, K., Vogel, S. N., Regan, M. W., et al. 2002, AJ, 124, 2581

Smith, D. A., Herter, T., Haynes, M. P., Beichman, C. A., & Gautier, III, T. N. 1996, ApJS, 104, 217

Solomon, P. M., Downes, D., & Radford, S. J. E. 1992, ApJL, 387, L55

Solomon, P. M., Downes, D., Radford, S. J. E., & Barrett, J. W. 1997, ApJ, 478, 144

Sorai, K., Nakai, N., Kuno, N., & Nishiyama, K. 2002, PASJ, 54, 179

Sosa-Brito, R. M., Tacconi-Garman, L. E., Lehnert, M. D., & Gallimore, J. F. 2001, ApJS, 136, 61

Spoon, H. W. W., Keane, J. V., Tielens, A. G. G. M., et al. 2002, A&A, 385, 1022

Spoon, H. W. W., Marshall, J. A., Houck, J. R., et al. 2007, ApJL, 654, L49

Strickland, D. K., Heckman, T. M., Colbert, E. J. M., Hoopes, C. G., & Weaver, K. A. 2004, ApJS, 151, 193

Surace, J. A., Sanders, D. B., & Evans, A. S. 2000, ApJ, 529, 170

Tennyson, J. 2005, *Astronomical spectroscopy : an introduction to the atomic and molecular physics of astronomical spectra*, Imperial College Press, London

Thean, A., Pedlar, A., Kukula, M. J., Baum, S. A., & O'Dea, C. P. 2000, MNRAS, 314, 573

Thomas, H. C., Dunne, L., Clemens, M. S., et al. 2002, MNRAS, 329, 747

Thomas, H. C., Dunne, L., Green, D. A., et al. 2004, MNRAS, 348, 1197

Thronson, Jr., H. A., Majewski, S., Descartes, L., & Hereld, M. 1990, ApJ, 364, 456

Thuan, T. X. 1984, ApJ, 281, 126

van Breugel, W., Filippenko, A. V., Heckman, T., & Miley, G. 1985, ApJ, 293, 83

van der Tak, F. F. S., Black, J. H., Schöier, F. L., Jansen, D. J., & van Dishoeck, E. F. 2007, A&A, 468, 627

Veilleux, S. & Osterbrock, D. E. 1987, ApJS, 63, 295

Veron, P., Goncalves, A. C., & Veron-Cetty, M.-P. 1997, A&A, 319, 52

Wang, M., Henkel, C., Chin, Y.-N., et al. 2004, A&A, 422, 883

Wernli, M., Wiesenfeld, L., Faure, A., & Valiron, P. 2007, A&A, 464, 1147

Wiedner, M. C., Wilson, C. D., Harrison, A., et al. 2002, ApJ, 581, 229

Wiedner, M., Wilson, C., Reid, M., Saito, M., & Menten, K. 2004, in *The Neutral ISM in Starburst Galaxies*, S. Aalto, S. Hüttemeister & A. Pedlar (Eds.), vol. 320 of *Astronomical Society of the Pacific Conference Series*, 35

Wynn-Williams, C. G. & Becklin, E. E. 1993, ApJ, 412, 535

Wyrowski, F., Schilke, P., & Walmsley, C. M. 1999, A&A, 341, 882

Zhang, J. S., Henkel, C., Kadler, M., et al. 2006, A&A, 450, 933

Zhi-yao, Y. 2003, MNRAS, 338, 745

Zink, E. C., Lester, D. F., Doppmann, G., & Harvey, P. M. 2000, ApJS, 131, 413

Appendix A

Oddities in Arp 220 and NGC 4418 – Bad Measurements or Variable HCN Intensity?

Together with the HC_3N, HNC and HCN measurements made by F. Costagliola which have been used in this work, some HCN 3-2 and HNC 3-2 measurements in a few galaxies were made. The main results of those measurements are yet to be published, however, as a correlation between the HC_3N luminosity and the HCN/HNC ratio seemed plausible, these spectra were investigated. For Arp 220, several such measurements already exist in the literature. When all these measurements were compared, something strange was detected in the intensities of the HCN 3-2 and HNC 3-2 lines – the different measurements showed quite some variation.

All HCN 3-2 data for Arp 220 found in the literature and from our measurements are shown in Table A.1, and the HNC 3-2 data are found in Table A.2. All intensities have been converted to fluxes to facilitate the comparison between measurements from different telescopes, as the flux should be independent of the choice of telescope. The conversion factors have been calculated from data given on the IRAM and JCMT websites together with formulae from Rohlfs & Wilson (2004). For IRAM, the conversion factor is 8.2 Jy/K for conversion from the $T_{\rm A}^*$ scale at 260 GHz. For JCMT, the conversion factor is 25.6 Jy/K for conversion from the $T_{\rm A}^*$ scale at 260 GHz.

For the articles where the temperature is given in $T_{\rm mb}$ and a main beam efficiency is given, this efficiency has been used for the conversion. If no efficiency is given, the efficiency has been obtained from the telescope websites. For IRAM, the main beam efficiency of today is $\eta_{\rm mb} = 0.59$, but for measurements performed before 2006 the older value of $\eta_{\rm mb} = 0.52$ should be used. For JCMT, $\eta_{\rm mb} = 0.69$ is used.

There is a notable difference between our intensity-to-flux conversion of the data in Krips et al. (2008) and the conversion made by Greve et al. (2009), the deviation being almost 25 %. I have not found any reasonable explanation for this error (e.g. a mix-up of temperature scales would produce a larger error). Thus, only the value calculated by us will be used below. Also, note that the values in Graciá-Carpio et al. (2008) and Krips et al. (2008) probably come from the same measurement, but nevertheless deviate by more than 20 %. If the values really come from the same measurement, this is an error that only the different methods of data reduction can account for.

Two persons reducing the same data would probably not get the exact same results, and a deviation of 20 % might be reasonable.

Table A.1. HCN 3-2 data for Arp 220

Reference	Telescope	Intensity [K km s^{-1}]	T scale	Flux [Jy km s^{-1}]	Obs. date
Wiedner et al. (2004)	JCMT 15 m	9.60[a]	$T_{\rm mb}$	170	Jun 2001
Greve et al. (2009)	JCMT 15 m	...		361 ± 73	Jan/Dec 2004
Cernicharo et al. (2006)	IRAM 30 m	8.2[a]	$T_{\rm A}^*$	67	Mar 2004
S. Martin-Ruiz[b]	IRAM 30 m	32.5 ± 0.6	$T_{\rm mb}$	157 ± 3	18 Sep 2005
S. Martin-Ruiz[b]	IRAM 30 m	34.9 ± 1.0	$T_{\rm mb}$	149 ± 4	31 Oct 2005
Graciá-Carpio et al. (2008)[c]	IRAM 30 m	18.04 ± 0.51	$T_{\rm A}^*$	148 ± 4	Dec 2005 - Nov 2006
Krips et al. (2008)[c]	IRAM 30 m	43.0 ± 1.0	$T_{\rm mb}$	183 ± 4	Jan/Aug 2006
Krips et al. (2008)[c,d]	IRAM 30 m	...		258 ± 77	Jan/Aug 2006
R. Hurley[b]	JCMT 15 m	6.78[a]	$T_{\rm A}^*$	174	17 Sep 2007
F. Costagliola[b]	IRAM 30 m	15.4 ± 0.3	$T_{\rm A}^*$	126 ± 2	Dec 2007

[a] Calculated from manual measurements in spectrum.
[b] Private communication (2009).
[c] These data probably come from the same measurements, although not stated in the articles (spectra are nearly identical).
[d] As converted by Greve et al. (2009).

The un-weighted average of the values in the table is 171 Jy km/s, even though the median value (157 Jy km/s) should be better for comparison in such a straggling sample. Six of the nine values lie in the quite narrow interval between 148 and 183 Jy km/s, which should be seen as a good error margin for extragalactic mm-wave spectroscopy (at least when assuming that the errors given by some of the references are greatly underestimated). Maybe even the interval 126 - 183 Jy km/s could be seen as acceptable in this context. However, two of the measurements are far outside even these rather generous boundaries, one of them showing more than twice as much intensity as the average, the other only 40 percent of the average.

Neither of these measurements is particularly noisy, so the problem should not be noise-related. The measurement with the highest flux is measured with JCMT, the one with the lowest is measured with IRAM, but there are acceptable measurements from both telescopes as well, so it does not seem to be a telescope issue either. It shall be noted, however, that Greve et al. (2009) note that they had a calibration problem with their HCN 3-2 measurements – the sideband ratio in the double sideband receiver was not unity, but varied with the local oscillator frequency. They although claim that this error has been corrected for properly.

Four of the Arp 220 HCN 3-2 spectra are shown in Figure A.2. Note that since they are taken with two different telescopes, and the temperature scales might be different, the actual peak amplitudes should not be compared – use Table A.1 for such a comparison. It can, however, be noted that not only the intensities, but also the line profiles, differ to some extent. In Cernicharo et al. (2006), the two peaks (corresponding to the eastern and western nuclei of the galaxy) are very hard to distinguish, but more or less of the same height. In the other three spectra, especially Krips et al. (2008) and Costagliola & Aalto (in prep.), the peak with the higher velocity is notably stronger than the other one.

Table A.2. HNC 3-2 data for Arp 220

Reference	Telescope	Intensity [K km s^{-1}]	T scale	Flux [Jy km s^{-1}]	Obs. date
Aalto et al. (2007b)	JCMT 15 m	18.6 ± 0.7	$T_{\rm mb}$	329 ± 12	Apr 2005
F. Costagliola[a]	IRAM 30 m	15.2 ± 0.1	$T_{\rm A}^*$	125 ± 1	Dec 2007
Aalto et al. (2009)	SMA	...		148 ± 29	Jun 2006

[a] Private communication (2009).

This is rather unexpected – generally molecular spectroscopic measurements of the same object and molecule should give the same values over time. There are nevertheless several possible explanations of this strange behaviour, basically split into two categories: Bad data or varying intensities. The data could be unreliable due to bad pointing, bad weather conditions during some of the runs or maybe that single-dish measurements are not reliable on such distant objects. The other possibility is more controversial – that the amount of dense gas would actually vary by tremendous amounts on time scales on the order of a few years.

There are relatively few molecular spectroscopy measurements made on extragalactic sources, and there is rarely more than one measurement available on a certain transition in a certain galaxy. Thus, it is not tested very well whether extragalactic molecular spectroscopy with single-dish measurements actually is repeatable, or if the differences between the measurement sessions are larger than what would be allowed for scientific data. The latter conclusion would of course reshape extragalactic astrochemistry as we know it – most earlier data would actually be useless (a detection should still be a detection, but the measured intensities should perhaps not be relied upon).

Being a bit more optimistic about data quality, going for the second possibility, that the HCN 3-2 line of Arp 220 actually is varying, there is instead a strange physical phenomenon to explain. This, however, seems unlikely, since the two most differing measurements (Greve et al. 2009, Cernicharo et al. 2006) both are measured the same year (2004). A time plot for all the HCN 3-2 measurements in Table A.1 can be found in Figure A.1.

The measurements on the spectral line HNC 3-2 in Arp 220 are much fewer in number – only two observations are found in the literature (Aalto et al. 2007b, Aalto et al. 2009). However, another measurement was performed by F. Costagliola in December 2007. The IRAM data taken by F. Costagliola agree well with the interferometric SMA data in Aalto et al. (2009), but disagree strongly with the JCMT data in Aalto et al. (2007b). The line profiles are in better agreement than for the HCN 3-2 line, but the integrated intensities differ by a factor of 2.5.

A similar behaviour is observed for NGC 4418, for which much less data are available. For this galaxy, however, the variations are only noticed in the HCN 3-2 line, not in the HNC 3-2 line, although the data origin from the same three references.

Quick investigations of several HCN transitions in galaxies where several such measurements are available indicate that this might not be isolated neither to these

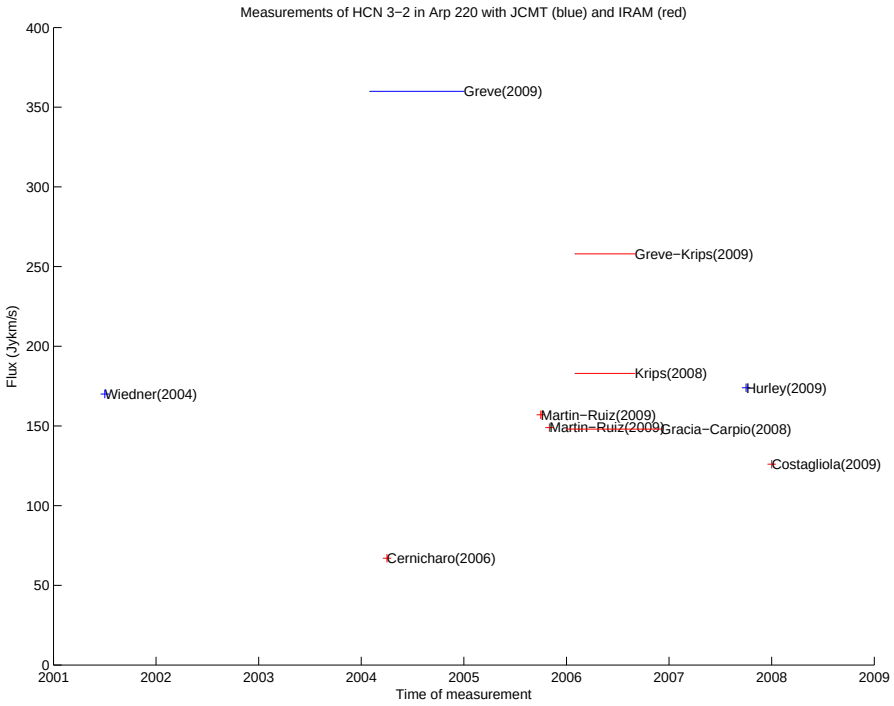

Figure A.1. Timeline for all measurements of HCN 3-2 found in Table A.1.

Table A.3. HCN 3-2 data for NGC 4418

Reference	Telescope	Intensity [K km s^{-1}]	T scale	Flux [Jy km s^{-1}]	Obs. date
Aalto et al. (2007b)	IRAM 30 m	5.2 ± 0.6	$T_{\rm mb}$	19.6 ± 2.2	May 2006
This work	IRAM 30 m	3.3 ± 0.7	$T_{\rm A}^*$	27.3 ± 2.5	Jun 2006
F. Costagliola[a]	IRAM 30 m	7.21 ± 0.27	$T_{\rm A}^*$	59.1 ± 2.2	Dec 2007

[a] Private communication (2009).

Table A.4. HNC 3-2 data for NGC 4418

Reference	Telescope	Intensity [K km s^{-1}]	T scale	Flux [Jy km s^{-1}]	Obs. date
Aalto et al. (2007b)	IRAM 30 m	10.8 ± 1	$T_{\rm mb}$	40.7 ± 3.8	May 2006
This work	IRAM 30 m	5.98 ± 0.77	$T_{\rm A}^*$	49.0 ± 6.3	Jun 2006
F. Costagliola[a]	IRAM 30 m	6.15 ± 0.26	$T_{\rm A}^*$	50.4 ± 2.1	Dec 2007

[a] Private communication (2009).

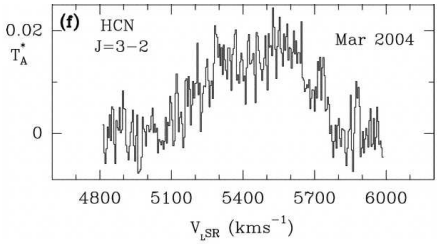

(a) Cernicharo et al. (2006)

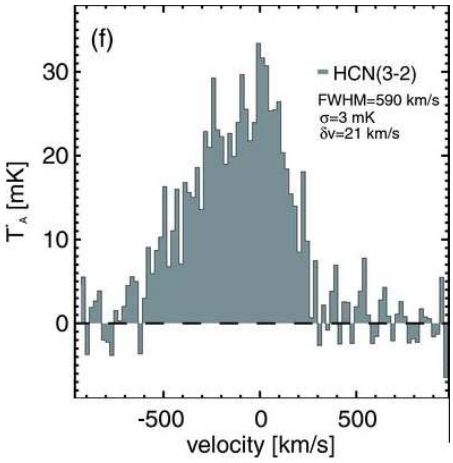

(b) Greve et al. (2009)

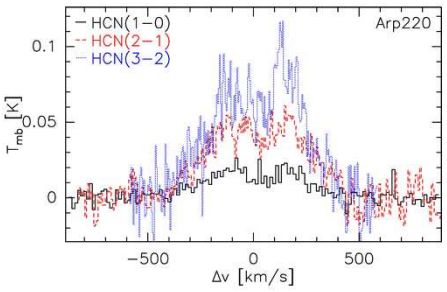

(c) Krips et al. (2008) (blue/upper line)

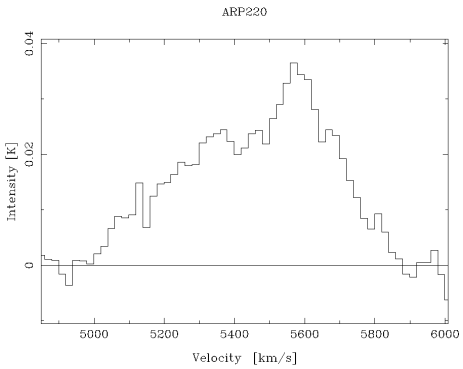

(d) Costagliola (private communication 2009)

Figure A.2. HCN 3-2 spectra in Arp 220

two galaxies, nor to this single transition. Arp 220 (Imanishi et al. 2007, Curran et al. 2000, Radford et al. 1991, Greve et al. 2009, Solomon et al. 1992, Krips et al. 2008, Graciá-Carpio et al. 2008), Mrk 273 (Imanishi et al. 2006a, Curran et al. 2000, Gao & Solomon 2004, Graciá-Carpio et al. 2008) and IRAS 17208-0014 (Imanishi et al. 2006a, Gao & Solomon 2004, Graciá-Carpio et al. 2008) all show large deviations in the available HCN 1-0 measurements, as well does Mrk 231 (Aalto et al. 2007b, Krips et al. 2008, Graciá-Carpio et al. 2008) and NGC 6240 (Krips et al. 2008, Greve et al. 2009, Graciá-Carpio et al. 2008) in HCN 3-2 and Arp 220 (Papadopoulos 2007, Wiedner et al. 2002, Greve et al. 2009) in HCN 4-3. The ratios between the largest and the smallest values found in the literature for each of these transitions lie around 2 or are even higher.

As Arp 220 is the galaxy for which the most data are available, more discrepancies will be found in this galaxy – this should not be taken as a sign of Arp 220 being a galaxy difficult to perform measurements on. Possibly, data on most other galaxies would show similar problems if only a sufficient number of measurements had been made.

Appendix B

Galaxy Classification Revisited

The difficulty of classifying active galaxies will be illustrated by comparing the classifications by H.W.W. Spoon, NED (2009) and careful evaluation of notes in NED (2009) for the galaxies in our sample. The classifications by Spoon come from Spoon et al. (2002) and from private communication (2009).

The evaluation of the NED notes were performed by browsing through the notes, searching for words like "starburst", "AGN", "Seyfert", "Sy", "active", etc., and investigating the articles found in this search, which led to conclusions towards the most plausible classification.

For clarity, when a galaxy is classified as being Sy1 or Sy2 (or anything in between, like Sy1.8) in the references, they have all been defined as AGNs below. For some galaxies, both AGN and starburst is suggested. In these cases, the references are investigated somewhat deeper, to establish if one of the classifications is more plausible than the other, or if the galaxy is a composite of AGN and starburst. For a further discussion on the different classifications, refer to Chapter 4.

As can be seen in Table B.1, the classifications from the three sources are far from identical. The clearest pattern seems to be that NED (2009) tends to define almost all objects as AGNs. This bias might be related to the source from where NED (2009) gets its classification, but the references for these classifications are not written out clearly. Upon contacting NED, they informed me that the classifications "come from the literature, but are not yet specifically referenced".

It can also be noted that the careful investigation of NED notes agree quite well with Spoon's classifications. A possible explanation is that he may have used the same approach for obtaining the classifications. The NED notes classification is the one used in this work, as shown in Table 5.2.

Table B.1. Galaxy classification

Galaxy	Spoon	NED (2009)	NED notes	NED notes reference
Arp 220	ULIRG	AGN	ULIRG, Obsc., SB?	Surace et al. (2000), Farrah et al. (2003)
Circinus	AGN	AGN	AGN (cp?)	Sosa-Brito et al. (2001)
IC 342	SB	AGN	SB	Förster Schreiber et al. (2004)
IC 694	-	SB, AGN	SB	Kinney et al. (1993)
IC 860	Normal	-	Obsc.	Lahuis et al. (2007)
I17208	ULIRG	SB	ULIRG, Obsc. (SB?)	Zink et al. (2000), Farrah et al. (2003)
M82	SB	SB	SB	Marcum et al. (2001)
Maffei 2	-	-	SB	Mason & Wilson (2004)
NGC 34	-	AGN	SB	Thean et al. (2000)
NGC 253	SB	SB/AGN	SB	Strickland et al. (2004)
NGC 613	SB	AGN	cp	Veron et al. (1997)
NGC 1056	-	AGN	AGN	Thean et al. (2000)
NGC 1068	AGN	AGN	cp	Papovich et al. (2003)
NGC 1365	AGN	AGN	cp	Reunanen et al. (2003)
NGC 1377	Obsc.	-	Obsc. AGN?	Imanishi (2006b)
NGC 1614	SB	AGN	SB	Lancon et al. (1996)
NGC 1808	AGN	AGN	SB (cp?)	Jungwiert et al. (1997), Lutz et al. (2004)
NGC 2146	SB	-	SB	Marcum et al. (2001)
NGC 2623	SB	AGN	SB	Smith et al. (1996)
NGC 3079	AGN	AGN	SB? AGN?	Sosa-Brito et al. (2001)
NGC 3256	SB	SB	SB	Kinney et al. (1993)
NGC 3690	-	-	SB	Conselice et al. (2000)
NGC 4418	Obsc.	AGN	Obsc. AGN?	Thomas et al. (2002)
NGC 4945	SB	AGN	SB (cp?)	Sosa-Brito et al. (2001)
NGC 5135	AGN	AGN	cp	Thuan (1984)
NGC 6946	-	AGN	SB	Alton et al. (1998)
NGC 7130	-	AGN	cp	Cid Fernandes et al. (1998)
UGC 5101	ULIRG	AGN	(U)LIRG, cp	Farrah et al. (2003)

Appendix C

Measured spectra

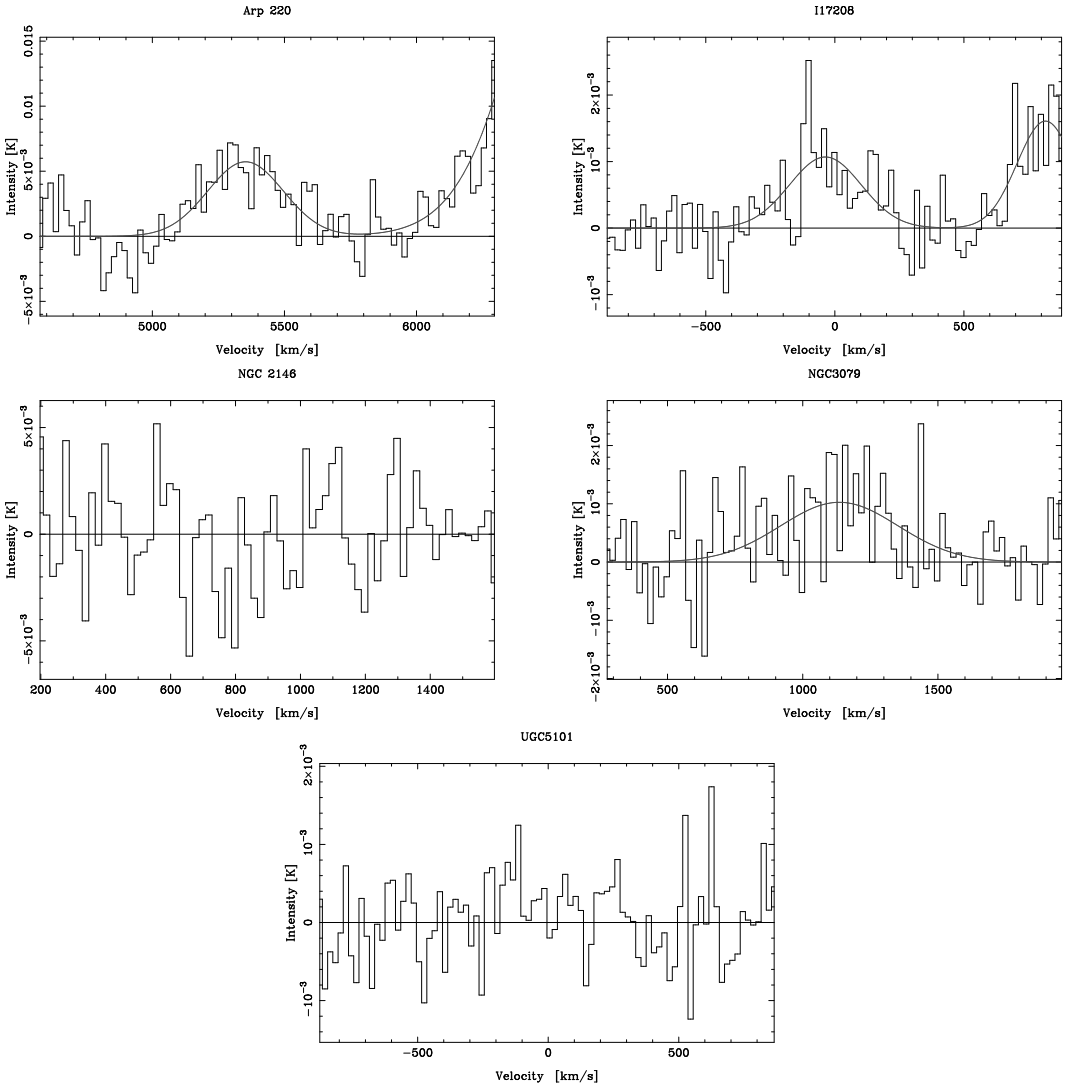

Figure C.1. HC_3N 10-9 spectra for Arp 220, I17208 (detections), NGC 2146 (non-detection), NGC 3079 (detection) and UGC 5101 (non-detection). For Arp 220 and I17208, part of the HNC 1-0 line is also visible. Note that some of the reported HC_3N 10-9-detections are found in the HNC 1-0 spectra, see Figures C.8-C.9.

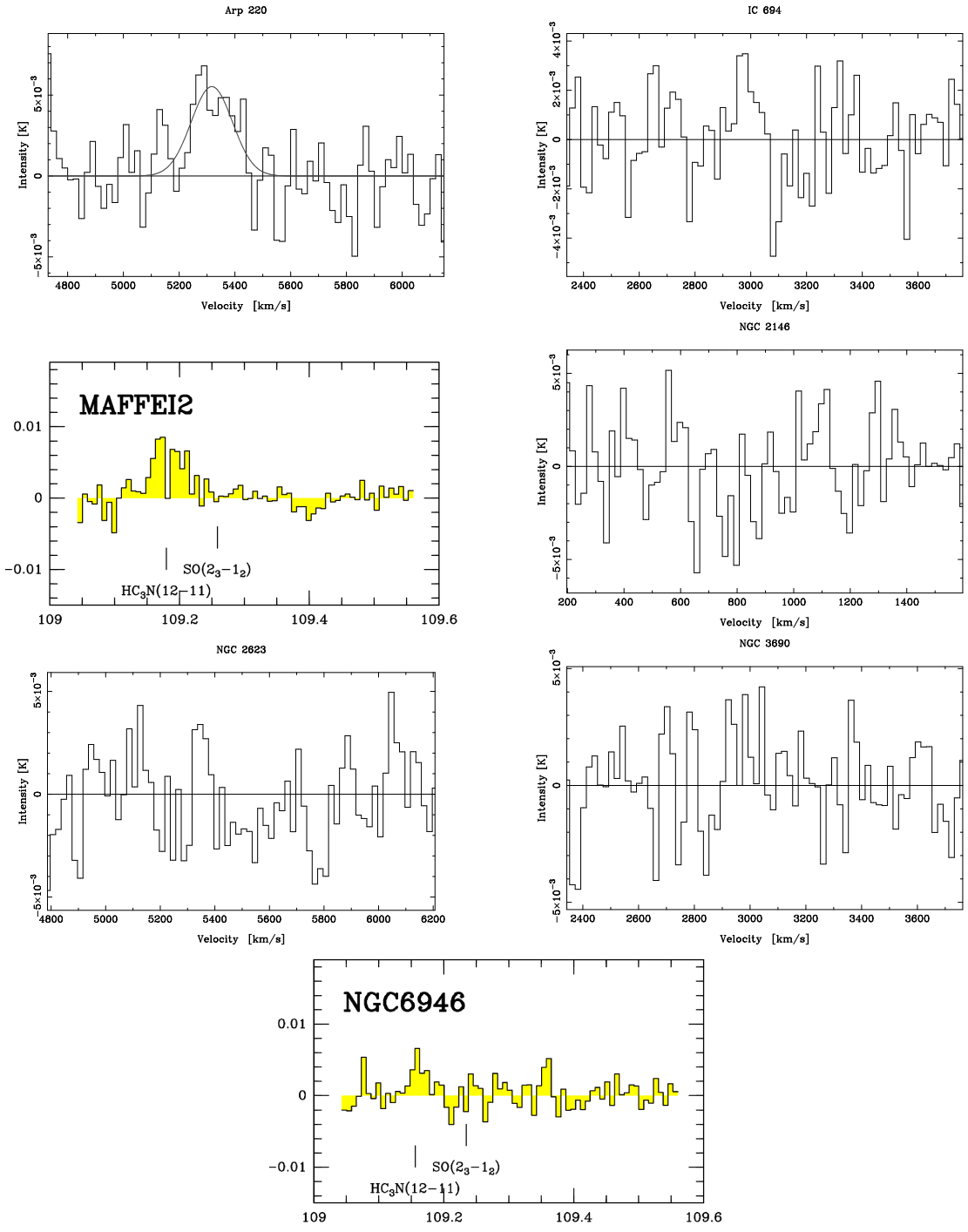

Figure C.2. HC_3N 12-11 spectra for Arp 220 (detection), IC 694 (non-detection), Maffei 2 (detection), NGC 2146, NGC 2623, NGC 3690 and NGC 6946 (non-detections).

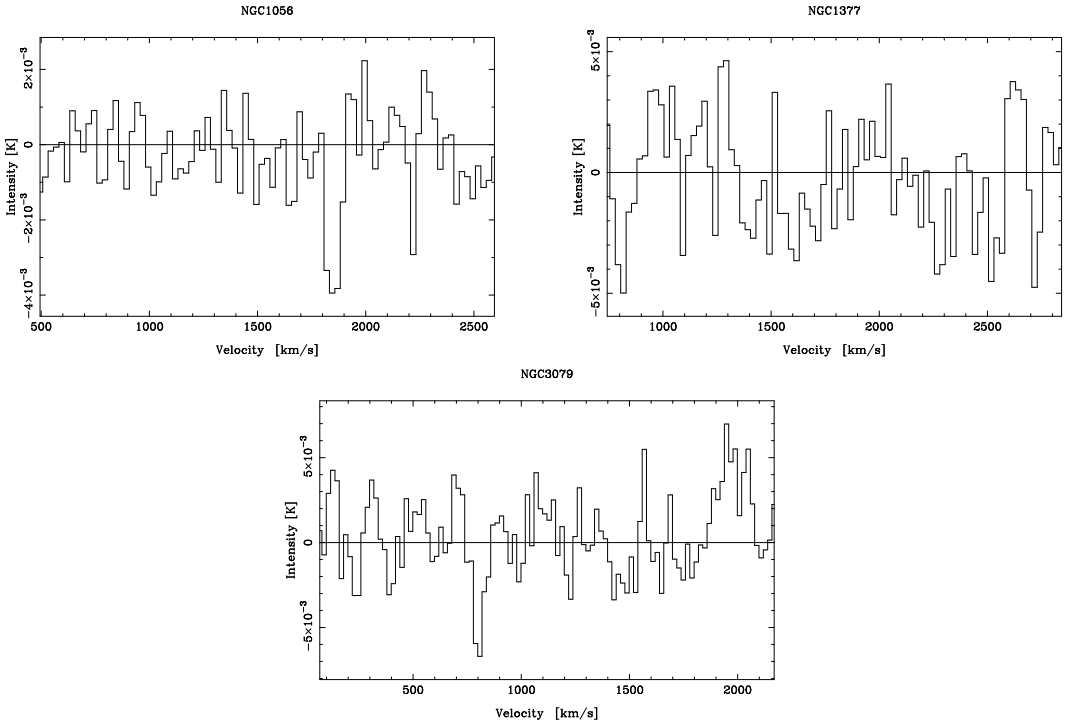

Figure C.3. HC_3N 16-15 spectra for NGC 1056, NGC 1377 and NGC 3079 (non-detections).

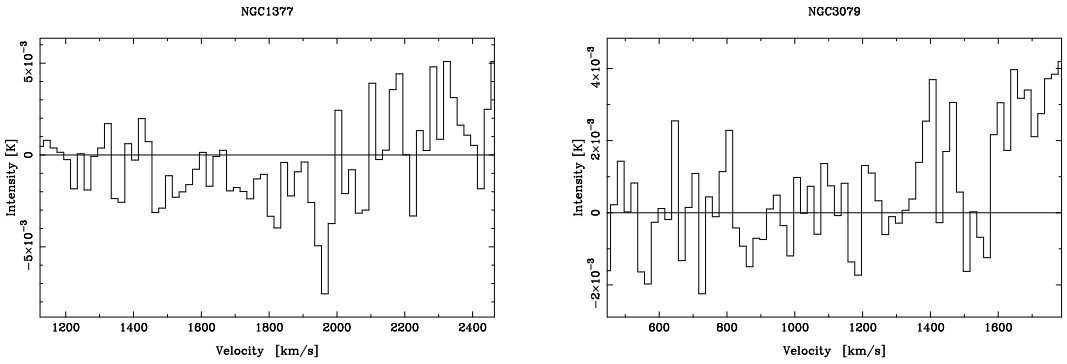

Figure C.4. HC_3N 25-24 spectra for NGC 1377 and NGC 3079 (non-detections).

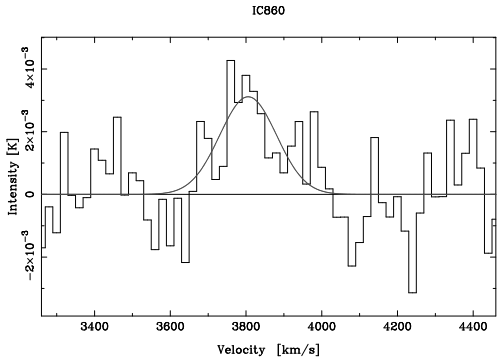

Figure C.5. HC_3N 28-27 spectrum for IC 860 (detection).

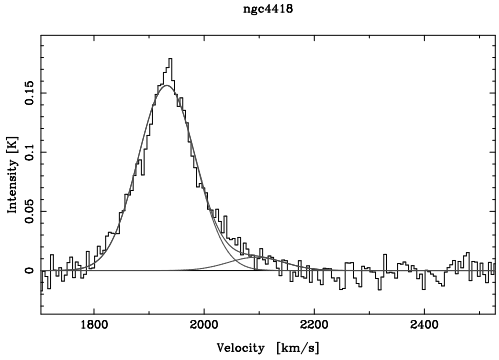

Figure C.6. CO 3-2 spectrum for NGC 4418. Tentative HC_3N 38-37 signal on the right hand side of the CO peak.

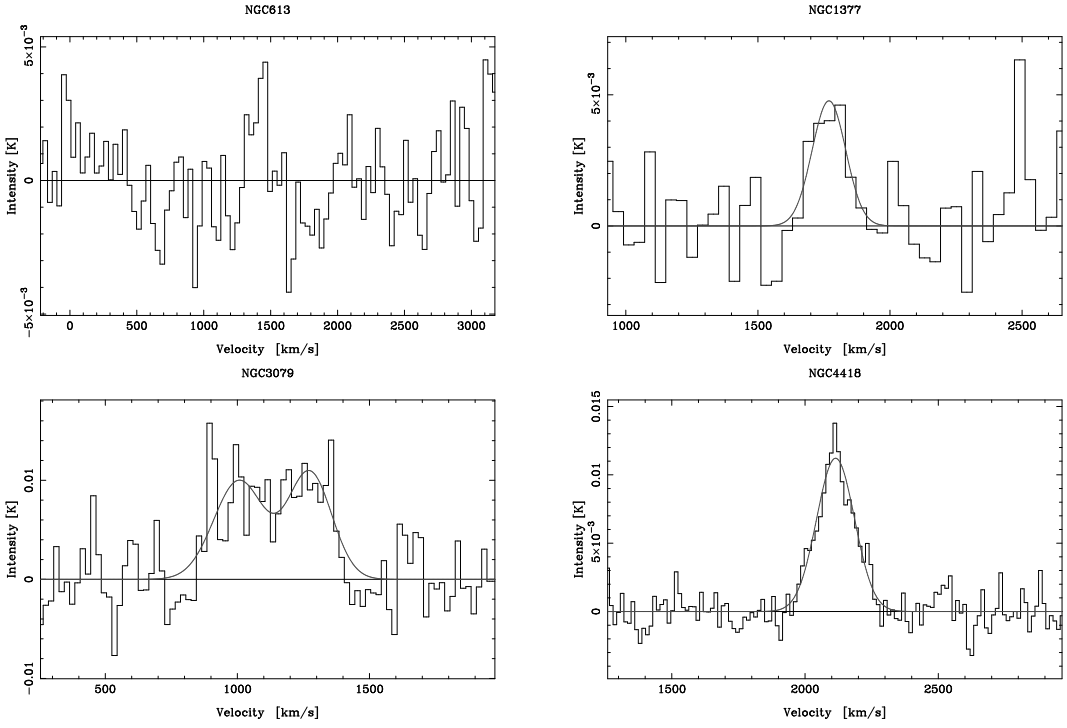

Figure C.7. HCN 1-0 spectra for NGC 613 (non-detection), NGC 1377, NGC 3079 and NGC 4418 (detections).

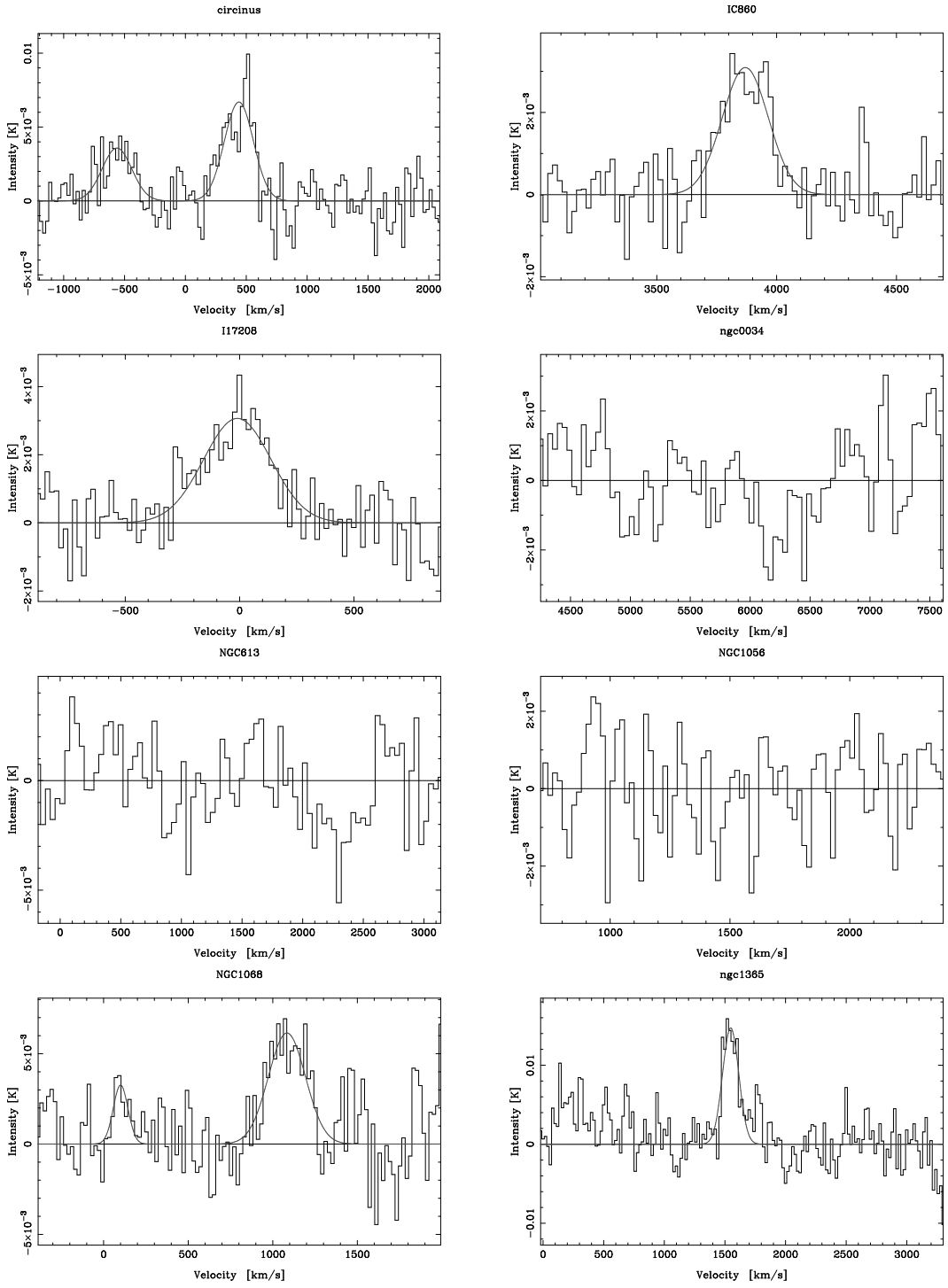

Figure C.8. HNC 1-0 spectra (first part) for Circinus, IC 860, I17208 (detections), NGC 34, NGC 613, NGC 1056 (non-detections), NGC 1068 and NGC 1365 (detections). For Circinus and NGC 1068, the HC_3N 10-9 line is also visible. Bandwidths for the spectra of NGC 34, NGC 613 and NGC 1365 are broad enough to include non-detections of the HC_3N 10-9 line, thus giving upper limits for these lines.

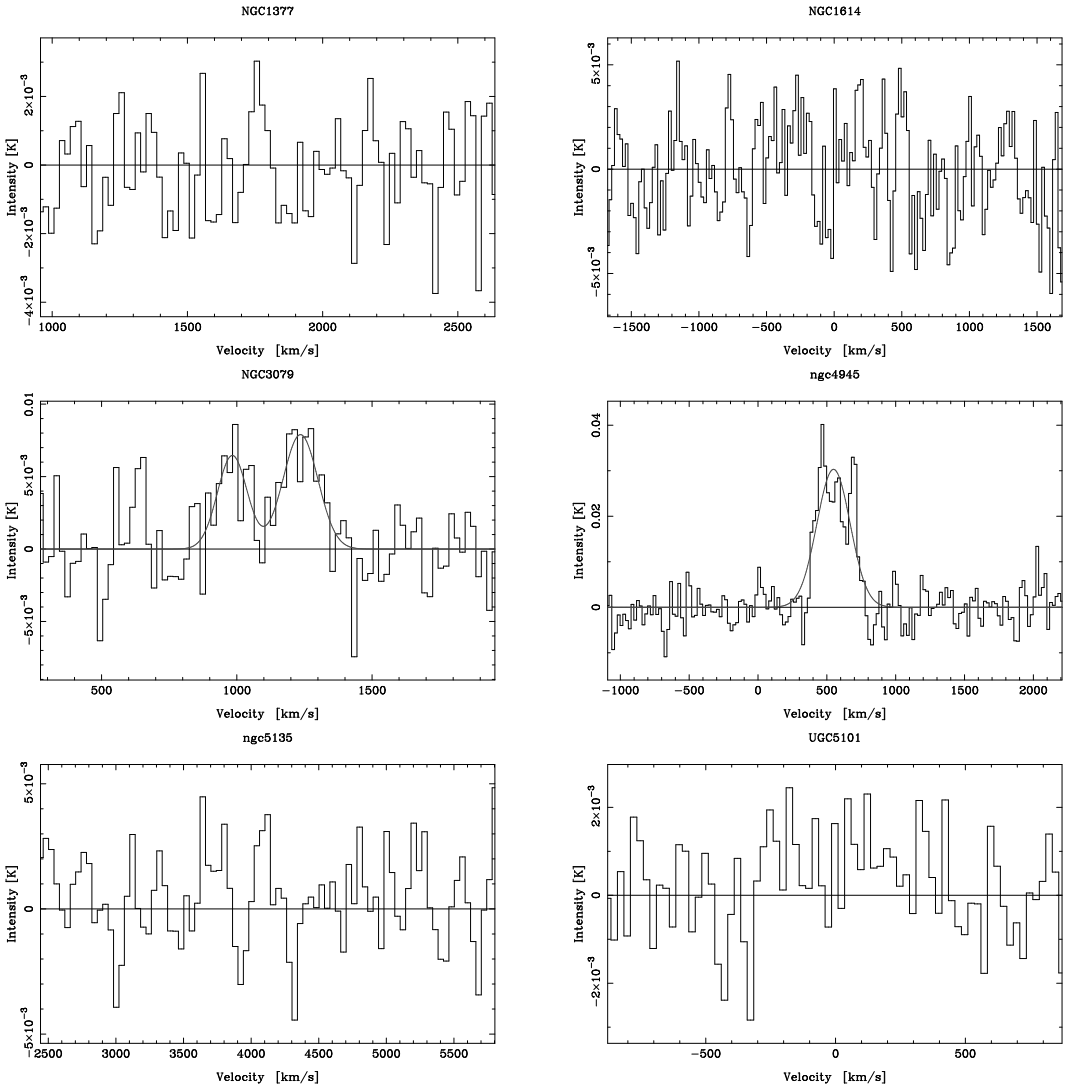

Figure C.9. HNC 1-0 spectra (cont.) for NGC 1377, NGC 1614 (non-detections), NGC 3079, NGC 4945 (detections), NGC 5135 and UGC 5101 (non-detections). Bandwidths for the spectra of NGC 1614 and NGC 5135 are broad enough to include non-detections of the HC_3N 10-9 line, thus giving upper limits for these lines.

Appendix D

Bestiary of Molecules

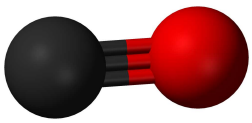

(a) The CO molecule

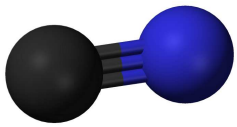

(b) The CN radical

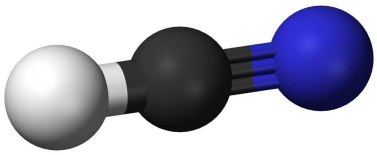

(c) The HCN molecule

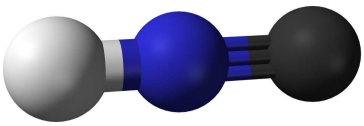

(d) The HNC molecule

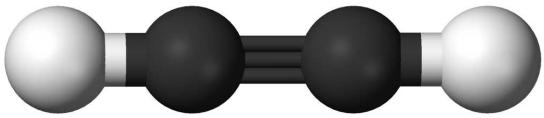

(e) The C_2H_2 molecule

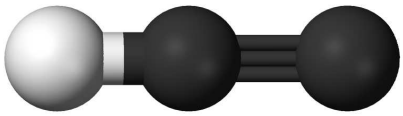

(f) The C_2H radical

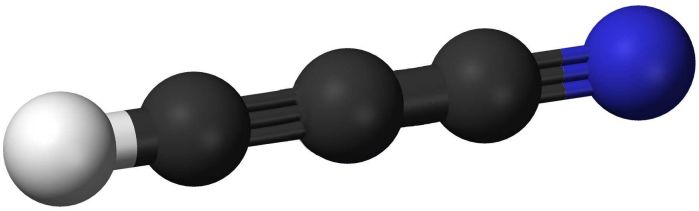

(g) The HC_3N molecule

Figure D.1. Bestiary of molecules. Atomic colours: Black - carbon; red - oxygen; white - hydrogen; blue - nitrogen. Image credit: Wikimedia Commons (used and manipulated under a creative commons license).

Appendix E

Methods used for the data analysis

The data analysis was performed with the software `xs`, developed by Per Bergman at Onsala Space Observatory.

The data reductions of spectra were carried out following the steps below:

1. Open the appropriate folder, filter the list to only contain measurements of a certain molecule in one galaxy.

2. Check all spectra manually for any odd features, like baseline shifts, uneven noise or separate channels with strong signals. Modify all spectra that have one or two erroneous channels – these channels are to be reduced to the average level of the spectrum. Remove all other spectra with odd features from further data reduction.

3. Fit a baseline of degree zero (a horizontal line) to the outer regions of each of the remaining spectra (baseline boxes should be drawn so that a potential spectral line is not included in this fitting). Subtract these baselines from each individual spectrum.

4. Average all spectra over system temperature and integration time, producing one single average spectrum.

5. Invert the scale on the x-axis, so that the velocity scale increases from left to right.

6. Reduce the spectral resolution to 25-35 km/s, to make any spectral lines appear more clearly,

7. Fit a baseline of degree one (a straight line) to the outer regions of the spectrum. This corrects for first-order baseline errors.

8. If a spectral line is seen, draw a moment box around it, making sure to include the full line. Draw baseline boxes around the rest of the spectrum. The spectral line intensity will now be given by the integrated area within the moment box. A Gaussian can be fitted to the line to give data such as the line width (full-width-half-maximum, FWHM) and amplitude of the peak.

9. If no spectral line is detected, an upper limit can still be determined. First, the expected line width must be known from another spectral line in the same galaxy (this assumes that the molecules have more or less the same distributions, which will give them the same line widths). Then, a moment box with this width is drawn where the line is expected to appear (normally in the centre of the spectrum). Draw baseline boxes around the rest of the spectrum. The rms per channel can now be found as the sigma for the baseline regions, giving the 2σ upper limit as $\frac{2 \cdot \mathrm{rms} \cdot \Delta v \cdot 1.067}{\sqrt{N}}$, where N is the number of channels in the moment box. The factor 1.067 comes from the fact that the area under a Gaussian with amplitude T and full width half maximum Δv approximately equals $1.067 \cdot T \Delta v$.